2018

Biophysics of cadherin interactions and junction assembly

Omer Shafraz
Iowa State University

Biophysics of cadherin interactions and junction assembly

by

Omer Lebbe M. Shafraz

A dissertation submitted to the graduate faculty

in partial fulfillment of the requirements for the degree of

DOCTOR OF PHILOSOPHY

Major: Physics

Program of Study Committee:
Sanjeevi Sivasankar, Major Professor
James Evans
John Lajoie
Xuefeng Wang
Robert Jernigan

The student author, whose presentation of the scholarship herein was approved by the program of study committee, is solely responsible for the content of this dissertation. The Graduate College will ensure this dissertation is globally accessible and will not permit alterations after a degree is conferred.

Iowa State University

Ames, Iowa

2018

DEDICATION

To my late father Omer Lebbe and mother Zaibunnisa,

To my wife Shifnaz and my little boy Ayaan.

TABLE OF CONTENTS

ACKNOWLEDGMENTS

I would like to thank everyone who was part of this journey with me. Most importantly, I would like to express my heartfelt gratitude to my advisor Dr. Sanjeevi Sivasankar for his incredible mentorship, continuous encouragement and valuable advice throughout my PhD. Sanjeevi, thank you for having me as a member of your lab and supporting me to present my work at various conferences that motivated me greatly in pursuing a scientific career.

I would also like to thank my program of study committee members Dr. James Evans, Dr. Robert Jernigan and Dr. Xuefeng Wang for their valuable time and feedback on my research.

Special thanks to Dr. John Lajoie and my lab mates Patrick Schmidt and Hussam Ibrahim for helping me with collecting data for the FRAP experiments using FPGA, for data analysis and valuable discussions.

I would also like to thank my collaborators, Dr. Molly Lowndes and Prof. James Nelson from Stanford University for making me a part of their JCS paper. Also, special thanks to Dr. Sara Stahley, Ms. Amber Caldara, and Prof. Andrew P. Kowalczyk at Emory University School of Medicine for their SIM data, Dr. Matthias Rübsam and Prof. Carien Niessen at University of Cologne for their confocal data that was included in this dissertation and in my manuscript.

I take this opportunity to thank past and present lab members. Specially Dr. Sabyasachi, Dr. Hui Li, Dr. Kristine Manibog and Dr. Chifu Yen for helping me from day one in the lab to understand the AFM, sample preparation and for their valuable suggestions and friendship. Also, I would like to thank Dr. Sunae Kim, Andrew Priest, Ramesh Koirala, Seth Heerschap and Benjamin Reichert for all the help and memorable times we have shared.

I would like to extend my sincere appreciation to my late father and mother for all their hard work, love and sacrifices. I also extend my appreciation towards my brother and sisters for sharing my responsibilities and letting me focus on my studies. I'm grateful to all the friends

who have been supportive in every good and bad moments. Last but not the least, my loving and supportive wife Shifnaz for her encouragements and patience, especially allowing me to work long nights and weekends in the lab and my cute little boy Ayaan for all the happiness and fun. Thank you all.

ABSTRACT

Desmosomes are robust cell adhesion junctions that are composed of two transmembrane desmosomal cadherin proteins: desmoglein (Dsg) and desmocollin (Dsc). The extracellular regions of Dsc and Dsg form an adhesive interface between cells while their cytoplasmic tails links to the intracellular keratin filament network. This dissertation investigates how Dsc and Dsg assemble into desmosomes using single molecule force measurements with an Atomic Force Microscope (AFM) and cell-based fluorescence assays. In Chapter 1, I give a brief over view of the content of this dissertation and the principles of AFM force measurements. In Chapter 2, I characterize the binding of isoform 2 of desmosomal cadherins. I show that Dsc2 dimerizes homophilically in a Ca^{2+} and tryptophan-2 (W2) dependent fashion; this binding mechanism, called 'strand-swap dimerization' has previously been found with other cadherins. In contrast, Dsg2 forms Ca^{2+} and W2 independent heterophilic binding with Dsc2. In Chapter 3 of the thesis, I describe how Dsg2 is recruited to desmosome. I show that E-cadherin (Ecad), a classical cadherin, interacts with Dsg2 in a Ca^{2+} independent manner, via a conserved Leu 175 on the Ecad *cis* binding interface. Furthermore, we demonstrate that desmosome assembly is initiated at sites of Ecad *trans* homodimerization and that Ecad-L175 is required for efficient Dsg2 and desmoplakin (DP) recruitment. Our data suggest that Ecad *trans* interactions at nascent cell-cell contacts initiate the recruitment of Dsg2 through direct *cis* interactions with Ecad; consequently, Dsg2 binds to Dsc2 and mediate robust desmosome assembly. In the fourth Chapter of this thesis, I develop and use a fast fluorescence recovery after photobleaching (FRAP) method to identify the dynamics of the Ecads trafficking at cell-cell junctions. Our preliminary data suggests that Ecads are recycled in and out of the junction by vesicle fusion. The final Chapter summarizes the conclusions and I propose future directions for these projects.

CHAPTER 1. INTRODUCTION

1.1 General Introduction

The goal of this dissertation is to enhance our understanding of desmosomal and classical cadherins using single molecule *in vitro* techniques and cell-based fluorescence techniques.

Cadherins are a family of cell adhesion proteins found in species ranging from unicellular organisms to mammals [1,2] where they are important for a variety of functions in tissue formation such as cell recognition, sorting, boundary formation and tissue maintenance[3–9] . Furthermore, cadherins are important in embryonic development[10–12], the plasticity and regulation of neuronal synapses[4,13], mechanotransduction [14–17] and cell signaling[18–21]. Defective cadherin expression caused by genetic and epigenetic modifications are linked to many diseases related to disruption of tissue architecture and tumors[22–28].

The cadherin superfamily[29] of cell-cell adhesion proteins are composed of four major subfamilies: classical cadherins, desmosomal cadherins, protocadherins and atypical cadherins [2,30]. Of these proteins, desmosomal cadherins and classical cadherins are essential for the maintenance of tissue integrity[31]. While classical cadherins mediate cell-cell adhesion in all soft tissues and play critical roles in tissue morphogenesis, desmosomal cadherins mediate robust cell-cell adhesion in tissues like the epidermis and heart which are exposed to significant levels of mechanical stress [32]. There are two types of desmosomal cadherins: desmoglein (Dsg) and desmocollin (Dsc), which are organized into four Dsg isoforms (Dsg1-4) and three Dsc isoforms (Dsc1-3) [33–35]. Of these isoforms, Dsg2 and Dsc2 are widely expressed in all layers of the epithelia and are also found in non-epithelial cells such as in the myocardium of the heart and lymph node follicles [36,37]. Ablation of Dsg2 results in embryonic lethality [38] while mutations in Dsg2 [39] and Dsc2 [40] cause arrhythmogenic right ventricular

cardiomyopathy (ARVC), a hereditary heart disease. In contrast isoforms 1 and 3 are restricted to complex epithelial tissues [41] and their loss of function leads to epidermal fragility, such as in the autoimmune blistering disease pemphigus [27,42,43]. Thus, it is important to have a greater understanding of these proteins. However, the exact molecular mechanism by which Dsc2 and Dsg2 binds and how they are incorporated into desmosome are not well understood. In Chapter 2 of this dissertation, I used single molecule AFM force spectroscopy combined with cellular based fluorescence methods to resolve the interaction of desmosomal cadherins. These experiments were carried out in collaboration with Dr. Sabyasachi Rakshit at Iowa State University; Dr. Molly Lowndes, Dr. Nicolas Borghi, and Prof. W. James Nelson at Stanford University; Dr. Robert Harmon and Prof. Kathleen Green at Northwestern University Feinberg School of Medicine.

Unlike desmosomal cadherins, classical cadherins are a much more extensively studied calcium-dependent transmembrane glycoproteins. The extracellular domains of classical cadherins from opposing cells, bind in a *trans* orientation to mediate adhesion. The cytoplasmic tails of classical cadherins interact with a range of effector proteins, most notably the catenins that link cadherins to the actin cytoskeleton [30,44]. Classical cadherins, which are subdivided into type I and type II, have extracellular regions that are comprised of five tandemly repeated extracellular (EC1-5) domains with three calcium binding sites in each interdomain linker [30]. Type I classical cadherins, which include epithelial (E) and neuronal (N) cadherin, have a conserved HAV tripeptide motif [45] and a conserved tryptophan 2 (Trp 2) residue [46] in the most distal EC (EC1). In contrast, type II classical cadherins, such as vascular endothelial (VE) cadherin, have two conserved Trps (Trp2 and Trp4) and also lack the HAV motif[47,48] . Several studies have shown that the classical cadherin E-cadherin (Ecad) promotes desmosome assembly. Immuno-electron micrographs demonstrate that Ecad localizes to the intercellular region of the bovine tongue epithelial desmosomes[49] . Blocking Ecad adhesion with antibodies delay desmosome formation in MDCK cells [50] and in human keratinocytes [51,52].

Desmosome formation in keratinocytes requires junctional initiation by the classical cadherins, Ecad or P-cadherin (Pcad) [53,54]. Similarly, live animal studies with classical cadherin-deficient mice show defective desmosome assembly [55].However, the precise molecular mechanism by which Ecads promote desmosome formation is unknown. In Chapter three, I combined AFM, super resolution microscopy and confocal fluorescence microscopy to characterize the interactions of Ecad, Dsg2 and Dsc2 and propose a model that explains how desmosome cadherins are incorporated into the desmosome assembly. These experiments were carried out in collaboration with Dr. Matthias Rübsam and Prof. Carien Niessen at the University of Cologne; Dr. Sara Stahley, Ms. Amber Caldara, and Prof. Andrew P. Kowalczyk at Emory University School of Medicine.

Adherens junctions, composed of classical cadherins, plays a prominent role in cell adhesion by linking cadherin–catenin protein complexes to the dynamic actin cytoskeleton [56]. These links are regularly rearranged by a variety of intra and extracellular signals, which subsequently change cadherin distribution at cell-cell junctions [57]. How cadherin junctional dynamics is regulated by the cell is not well established. While Fluorescence Recovery After Photobleaching (FRAP) can be used to determine these dynamic events, conventional FRAP lacks the temporal resolution to determine fast dynamics. In Chapter four, using a custom built confocal microscopy set up [58], I explore rapid cadherin dynamics to determine the prominent mechanism involved in cellular junction modulation. These experiments are being carried out in collaboration with Mr. Hussam Ibrahim, Mr. Patrick Schmidt and Prof. John Lajoie at Iowa State University.

1.2 Thesis Organization

My dissertation is organized as follows:

In Chapter 1, I give a general introduction to desmosomal and classical cadherins and explain about the principles of an AFM and how it is used in single molecule force measurements.

The second Chapter describes the binding properties of desmosomal cadherins measured using single molecule AFM and immunofluorescence data that was published in Journal of Cell Science [59] in 2014. While Dr. Rakshit and I measured the binding properties of desmosomal cadherins using AFM, our collaborator Dr. Lowndes from Prof. Nelson's lab (Stanford University) obtained the immunofluorescence data. In this study we showed that Dsc2 forms both homophilic interactions in the presence of Ca^{2+} via Trp-2 (W2) mediated strand swapping, and heterophilic interactions with Dsg2 in a Ca^{2+} independent fashion. In contrast Dsg2 only participates in heterotypic binding. Using cell-based assays, our collaborators showed that Dsc2, but not Dsg2, is sufficient to induce the recruitment of desmosome-specific cytoplasmic protein desmoplakin (DP) into punctate cellular structures. Mutants expressed in the cells showed that Dsg2 is incorporated in desmosome by an unknown W2 independent mechanism.

In the third Chapter, I investigate how Dsg2 is recruited to desmosomes. This chapter is a manuscript that has been submitted to eLife in 2018. Previous studies have shown that Ecad is necessary to desmosome formation. Here, I identified an important amino acid (Leu 175) in Ecad that is essential to bring in Dsg2 to desmosome using AFM force measurements. Our collaborators Dr. Stahley and Ms. Caldara from Prof. Kowalczyk's lab (Emory University) used immunofluorescence structured illumination microscopy (SIM) to show that Ecad is present in early desmosome and it is excluded as desmosome matures. Our collaborators Dr. Rübsam and Prof. Niessen (University of Cologne) used confocal microscopy to show that desmosome assembly is initiated at sites of Ecad *trans* homodimerization and that Ecad-L175 is required for efficient Dsg2 and DP recruitment to sites of early intercellular contact formation. Taken together, our data indicates that Ecad *trans* interactions at nascent cell-cell contacts initiate the recruitment of Dsg through direct *cis* interactions with Ecad which facilitates desmosome assembly.

Chapter four describes recently collected data by using FRAP to understand how Ecad is trafficked in and out of cell-cell junctions. Using an avalanche photodiode (APD) based detection scheme, we increased our time resolution to μs and have obtained preliminary results that suggest that Ecads are recycled to the junction primarily by endocytosis, not membrane diffusion.

Finally, Chapter 5 summarizes the conclusions of this dissertation and its significance in understanding the role of desmosomal cadherins and classical cadherins. I also propose future direction for these projects.

1.3 Single Molecule Force Spectroscopy: Theory and Method

1.3.1 Principles of atomic force microscope

Single molecule force measurement with an AFM is widely used to probe the molecular interactions between a ligand and a receptor. In AFM, a cantilever mounted onto a piezo electric translator can be moved towards and away from the substrate. The cantilever behaves like a Hookean spring where the force sensed by the cantilever is,

$$F=K_c.\ \delta z\ ; \qquad (1)$$

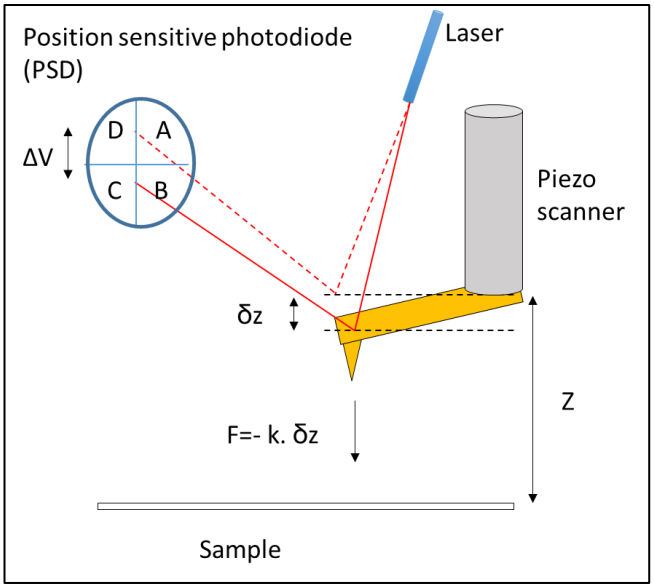

Figure 1.1 Schematic diagram of an Atomic Force Microscope (AFM)

where K_c is spring constant and δz deflection of the cantilever (Figure 1.1). The deflection of the cantilever (δz), is obtained from the change of position of a laser beam that is reflected off the back of the cantilever onto a Quadrant Photodiode (QPD). The QPD has four quadrants where the voltage signal from each quadrant is A, B, C and D (Figure 1.1). Change in voltage corresponding to δz is,

$$\Delta V = (A+D)-(C+B)/(A+B)+(C+D). \quad (2)$$

ΔV is related to the deflection δz using the optical lever sensitivity measured from the calibration curve of the cantilever (Figure 1.2 A) [60–62].

1.3.2 Cantilever sensitivity measurement

The optical lever sensitivity is measured for each cantilever using the slope (S) of the V vs Z_p (relative piezo translator displacement) curve (Figure 1.2 A). An approach and a retraction curve are completed by applying a high force on a hard, non-deformable surface. The region where the V is linear to Z_p is fit to a straight line and from the fit, S is determined[60–62].

$$\Delta V=-1/S \quad (3)$$

1.3.3 Spring constant of the cantilever

The spring constant is determined by using the thermal fluctuations method proposed by Hutter and Bechhofer[63,64]. In this analysis, the free cantilever is assumed to be an ideal spring with mass *m* and resonant frequency ω_0, modeled as a 1-D harmonic oscillator that is fluctuating in response to the thermal noise. For a cantilever with z_0 vertical oscillation,

$$\tfrac{1}{2}\, m\, \omega_0^2 = \tfrac{1}{2}\, K_c < z_0^{\,2} >; \quad (4)$$

From the equipartition theorem, the average energy in 1-D is $\tfrac{1}{2}\, k_B T$, where k_B-Boltzmann constant, T-Absolute temperature. Hence,

$$K_c < z_0^{\,2} > = k_B T; \quad (5)$$

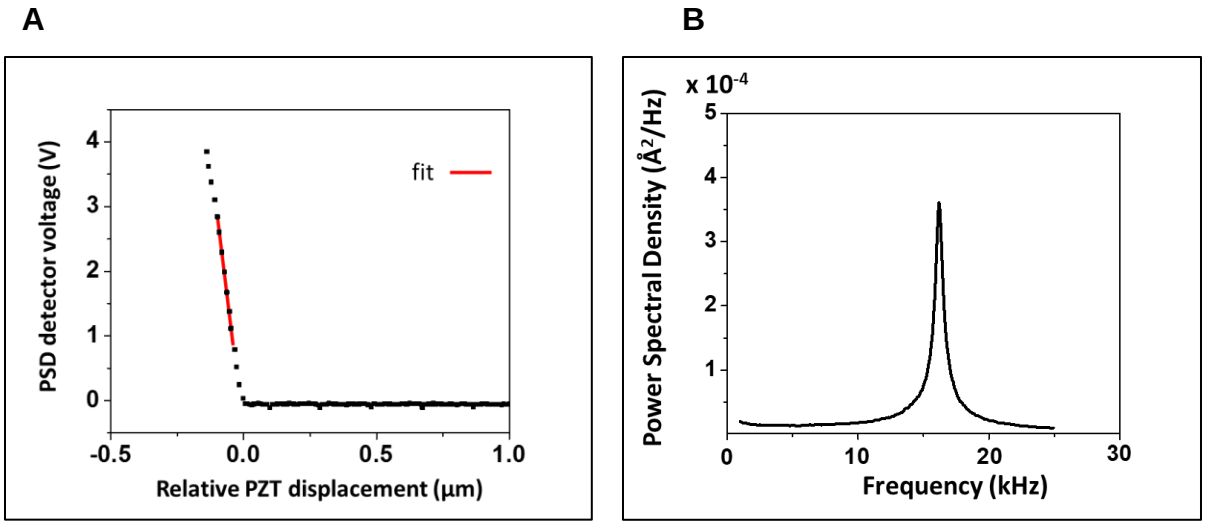

Figure 1.2 (A) Example calibration curve used to determine the cantilever sensitivity, (B) power spectrum density of a freely oscillating cantilever.

$< z_0^2 >$ is calculated from the area under the Lorentzian curve fitted to the power spectrum density of the freely oscillating cantilever (Figure 1.2 B).

1.3.4 Force measurement

In a typical experiment, proteins are attached to Poly Ethylene Glycol (PEG) polymer tethers functionalized on substrates and AFM cantilevers. At the start of the experiment, the AFM cantilever and substrate decorated with proteins are brought into contact to allow opposing proteins to interact. The tip is then withdrawn from the substrate and the force required to rupture the adhesive complex is measured. Interaction of molecules immobilized on the AFM cantilever and substrate results in unbinding events characterized by non-linear stretching of the PEG tethers (Figure 1.3 A); the stretching of PEG serves as a molecular fingerprint for single molecule unbinding, since its extension under force has been well characterized [65]. These force extension curves are used to identify binding partners and to estimate their kinetic properties. No such strechting is observed in the absence of a molecular binding interaction (Figure 1.3 B).

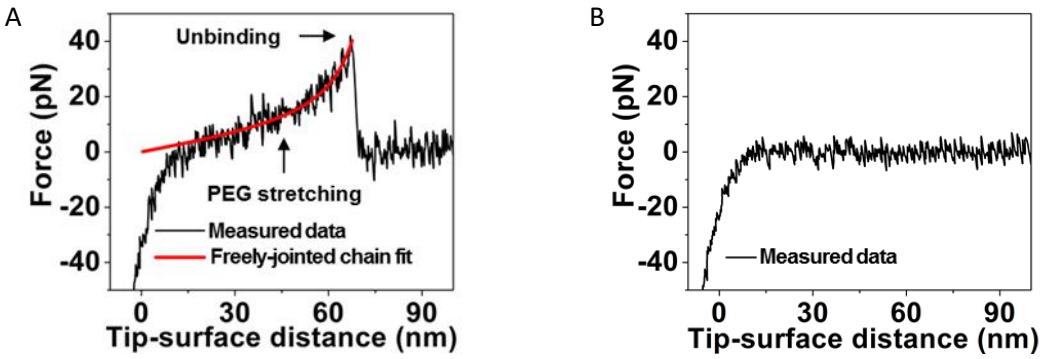

Figure 1. 3 (A) A single molecule binding event shows the extension of the PEG (black line) and extended FJC fitting using total least squares fit (red line) and (B) no any interaction.

The region of PEG stretching in each unbinding force curve is fit to an extended freely jointed chain model (Eq. 6) [65] using a total least square fitting protocol.

$$L(F) = L_c(F)\left(coth\left(\frac{FL_k}{k_BT}\right) - \frac{k_BT}{FL_k}\right) + \frac{F}{K_s} \qquad (6)$$

Where the $\mathrm{L_c}$ contour length, kuhn length $\mathrm{L_k}$ and the chain stiffness per monomer $\mathrm{K_s}$.

The contour length L_c of the PEG tethers is determined from the fits. The histogram of L_c for each experiment is fit to a Gaussian distribution and only force curves that had a L_c within one standard deviation from the center are accepted for further analysis.

The loading rate r_f for each curve was calculated using (Eq. 7) [66]

$$\frac{1}{r_f} = \frac{1}{k_c v}\left(1 + \frac{k_c L_c}{l_k}\left(\left(\frac{l_k}{F}\right)^2 - \mathrm{csch}^2\left(\frac{F}{l_k}\right)\right)\right) \qquad (7)$$

where k_c is the spring constant of the cantilever, F is the unbinding force and v is the pulling speed.

Protein concentrations on the surfaces are carefully tuned such that the binding probability measured is ~5-6 %. This low binding rate allows 97% of the observed interactions to be single molecule interactions.

1.3.5 Dynamic force spectroscopy

Specific interaction of biomolecules arises from formation of multiple non-covalent bonds such as hydrogen bonds and ionic bonds. Two interacting partner molecules have to overcome an activation barrier ΔG (Figure 1.4) before they unbind. The unbinding rate driven by thermal fluctuation is,

$$k_{off} = \omega \, exp\left(\frac{-\Delta G}{k_B T}\right); \qquad (8)$$

where k_{off}-intrinsic off rate, ω- frequency of attempts to cross the barrier k_B-boltzmann constant, T-absolute temperature.

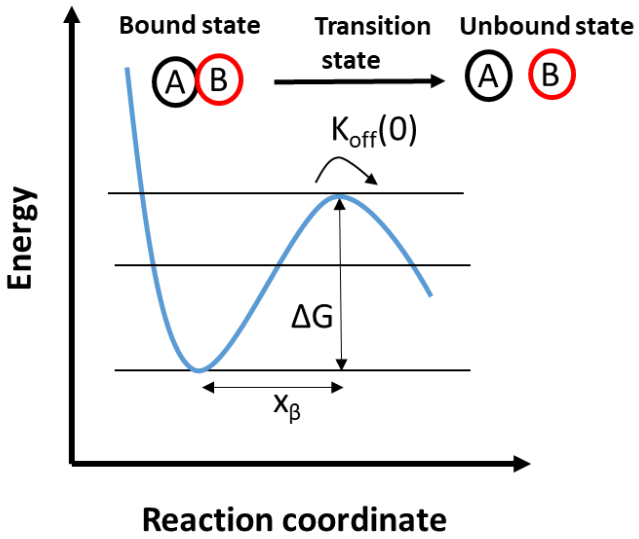

Figure 1.4 Energy diagram for bound molecules A and B have to cross the barrier gap ΔG to unbind. ΔG is lowered up on applied force.

Bell [67] showed that barrier is lowered under the force (F) applied along the direction of the reaction coordinate (Figure 1.4, Eq 9) such that,

$$\Delta G(F) = \Delta G - F.x_\beta \qquad (9)$$

where x_β -the width of the potential energy barrier. Now the off rate is force dependent,

$$k_{off} = k_{off}(0) exp\left(\frac{-(\Delta G - F.x_\beta).}{k_B T}\right); \quad (10)$$

Evans and Ritchie[68] extended Bell's theory to Bell-Evans model:

$$F^* = \frac{k_B T}{x_\beta} ln\left(\frac{r_f x_\beta}{k_B T\, k_{off}^0}\right) \; ; \quad (11)$$

where F^* mean rupture force, r_f loading rate. This model predicts that rupture force linearly increases with logarithm of the rate of application of force. From the linear fit to plot of F^* vs. r_f , intrinsic lifetime ($1/k_{off}^0$) of the molecular interaction can be determined.

1.4 References

1. Gul, I. S., Hulpiau, P., Saeys, Y. & van Roy, F. Evolution and diversity of cadherins and catenins. *Exp. Cell Res.* **358,** 3–9 (2017).

2. Hulpiau, P. & van Roy, F. Molecular evolution of the cadherin superfamily. *Int. J. Biochem. Cell Biol.* **41,** 349–369 (2009).

3. Halbleib, J. M. & Nelson, W. J. Cadherins in development: cell adhesion, sorting, and tissue morphogenesis. *Genes Dev.* **20,** 3199–3214 (2006).

4. Gumbiner, B. M. Regulation of cadherin-mediated adhesion in morphogenesis. *Nat. Rev. Mol. Cell Biol.* **6,** 622–634 (2005).

5. Niessen, C. M. & Gumbiner, B. M. Cadherin-mediated cell sorting not determined by binding or adhesion specificity. *J. Cell Biol.* **156,** 389–399 (2002).

6. Perez, T. D. & Nelson, W. J. Cadherin adhesion: mechanisms and molecular interactions. *Handb Exp Pharmacol* 3–21 (2004). doi:10.1007/978-3-540-68170-0_1

7. Maître, J.-L. & Heisenberg, C.-P. Three functions of cadherins in cell adhesion. *Curr. Biol.* **23,** R626–33 (2013).

8. Angst, B. D., Marcozzi, C. & Magee, A. I. The cadherin superfamily: diversity in form and function. *J. Cell Sci.* **114,** 629–641 (2001).

9. Priest, A. V., Shafraz, O. & Sivasankar, S. Biophysical basis of cadherin mediated cell-cell adhesion. *Exp. Cell Res.* **358,** 10–13 (2017).

10. Kan, N. G. *et al.* Gene replacement reveals a specific role for E-cadherin in the formation of a functional trophectoderm. *Development* **134,** 31–41 (2007).

11. Larue, L., Ohsugi, M., Hirchenhain, J. & Kemler, R. E-cadherin null mutant embryos fail to form a trophectoderm epithelium. *Proc. Natl. Acad. Sci. USA* **91,** 8263–8267 (1994).

12. Radice, G. L. *et al.* Developmental defects in mouse embryos lacking N-cadherin. *Dev. Biol.* **181,** 64–78 (1997).

13. Williams, M. E. *et al.* Cadherin-9 regulates synapse-specific differentiation in the developing hippocampus. *Neuron* **71,** 640–655 (2011).

14. Leckband, D. E. & de Rooij, J. Cadherin adhesion and mechanotransduction. *Annu. Rev. Cell Dev. Biol.* **30,** 291–315 (2014).

15. Kazmierczak, P. *et al.* Cadherin 23 and protocadherin 15 interact to form tip-link filaments in sensory hair cells. *Nature* **449,** 87–91 (2007).

16. Barry, A. K., Wang, N. & Leckband, D. E. Local VE-cadherin mechanotransduction triggers long-ranged remodeling of endothelial monolayers. *J. Cell Sci.* **128,** 1341–1351 (2015).

17. Sotomayor, M., Weihofen, W. A., Gaudet, R. & Corey, D. P. Structure of a force-conveying cadherin bond essential for inner-ear mechanotransduction. *Nature* **492,** 128–132 (2012).

18. Harris, T. J. C. & Tepass, U. Adherens junctions: from molecules to morphogenesis. *Nat. Rev. Mol. Cell Biol.* **11,** 502–514 (2010).

19. Harris, T. J. C. An introduction to adherens junctions: from molecular mechanisms to tissue development and disease. *Subcell. Biochem.* **60,** 1–5 (2012).

20. Muhamed, I. *et al.* E-cadherin-mediated force transduction signals regulate global cell mechanics. *J. Cell Sci.* **129,** 1843–1854 (2016).

21. Perez, T. D., Tamada, M., Sheetz, M. P. & Nelson, W. J. Immediate-early signaling induced by E-cadherin engagement and adhesion. *J. Biol. Chem.* **283,** 5014–5022 (2008).

22. Hajra, K. M. & Fearon, E. R. Cadherin and catenin alterations in human cancer. *Genes Chromosomes Cancer* **34,** 255–268 (2002).

23. Ashaie, M. A. & Chowdhury, E. H. Cadherins: The Superfamily Critically Involved in Breast Cancer. *Curr. Pharm. Des.* **22,** 616–638 (2016).

24. Resink, T. J., Philippova, M., Joshi, M. B., Kyriakakis, E. & Erne, P. Cadherins and cardiovascular disease. *Swiss Med Wkly* **139,** 122–134 (2009).

25. Pinho, S. S. *et al.* Role of E-cadherin N-glycosylation profile in a mammary tumor model. *Biochem. Biophys. Res. Commun.* **379,** 1091–1096 (2009).

26. Kant, S., Holthöfer, B., Magin, T. M., Krusche, C. A. & Leube, R. E. Desmoglein 2-Dependent Arrhythmogenic Cardiomyopathy Is Caused by a Loss of Adhesive Function. *Circ Cardiovasc Genet* **8,** 553–563 (2015).

27. Amagai, M. & Stanley, J. R. Desmoglein as a target in skin disease and beyond. *J. Invest. Dermatol.* **132,** 776–784 (2012).

28. Berx, G. & van Roy, F. Involvement of members of the cadherin superfamily in cancer. *Cold Spring Harb. Perspect. Biol.* **1,** a003129 (2009).

29. Nollet, F., Kools, P. & van Roy, F. Phylogenetic analysis of the cadherin superfamily allows identification of six major subfamilies besides several solitary members. *J. Mol. Biol.* **299,** 551–572 (2000).

30. Brasch, J., Harrison, O. J., Honig, B. & Shapiro, L. Thinking outside the cell: how cadherins drive adhesion. *Trends Cell Biol.* **22,** 299–310 (2012).

31. Rübsam, M. *et al.* Adherens junctions and desmosomes coordinate mechanics and signaling to orchestrate tissue morphogenesis and function: an evolutionary perspective. *Cold Spring Harb. Perspect. Biol.* (2017). doi:10.1101/cshperspect.a029207

32. Dusek, R. L., Godsel, L. M. & Green, K. J. Discriminating roles of desmosomal cadherins: beyond desmosomal adhesion. *J. Dermatol. Sci.* **45,** 7–21 (2007).

33. Saito, M., Tucker, D. K., Kohlhorst, D., Niessen, C. M. & Kowalczyk, A. P. Classical and desmosomal cadherins at a glance. *J. Cell Sci.* **125,** 2547–2552 (2012).

34. Nuber, U. A., Schäfer, S., Schmidt, A., Koch, P. J. & Franke, W. W. The widespread human desmocollin Dsc2 and tissue-specific patterns of synthesis of various desmocollin subtypes. *Eur. J. Cell Biol.* **66,** 69–74 (1995).

35. Koch, P. J., Goldschmidt, M. D., Zimbelmann, R., Troyanovsky, R. & Franke, W. W. Complexity and expression patterns of the desmosomal cadherins. *Proc. Natl. Acad. Sci. USA* **89,** 353–357 (1992).

36. Getsios, S., Huen, A. C. & Green, K. J. Working out the strength and flexibility of desmosomes. *Nat. Rev. Mol. Cell Biol.* **5,** 271–281 (2004).

37. Delva, E., Tucker, D. K. & Kowalczyk, A. P. The desmosome. *Cold Spring Harb. Perspect. Biol.* **1,** a002543 (2009).

38. Eshkind, L. *et al.* Loss of desmoglein 2 suggests essential functions for early embryonic development and proliferation of embryonal stem cells. *Eur. J. Cell Biol.* **81,** 592–598 (2002).

39. Awad, M. M. *et al.* DSG2 mutations contribute to arrhythmogenic right ventricular dysplasia/cardiomyopathy. *Am. J. Hum. Genet.* **79,** 136–142 (2006).

40. Syrris, P. *et al.* Arrhythmogenic right ventricular dysplasia/cardiomyopathy associated with mutations in the desmosomal gene desmocollin-2. *Am. J. Hum. Genet.* **79,** 978–984 (2006).

41. Green, K. J. & Simpson, C. L. Desmosomes: new perspectives on a classic. *J. Invest. Dermatol.* **127,** 2499–2515 (2007).

42. Samuelov, L. *et al.* Desmoglein 1 deficiency results in severe dermatitis, multiple allergies and metabolic wasting. *Nat. Genet.* **45,** 1244–1248 (2013).

43. Amagai, M. Autoimmune and infectious skin diseases that target desmogleins. *Proc. Jpn. Acad. Ser. B. Phys. Biol. Sci.* **86,** 524–537 (2010).

44. Weis, W. I. & Nelson, W. J. Re-solving the cadherin-catenin-actin conundrum. *J. Biol. Chem.* **281,** 35593–35597 (2006).

45. Blaschuk, O. W., Sullivan, R., David, S. & Pouliot, Y. Identification of a cadherin cell adhesion recognition sequence. *Dev. Biol.* **139,** 227–229 (1990).

46. Shapiro, L. *et al.* Structural basis of cell-cell adhesion by cadherins. *Nature* **374,** 327–337 (1995).

47. Shapiro, L. & Weis, W. I. Structure and biochemistry of cadherins and catenins. *Cold Spring Harb. Perspect. Biol.* **1,** a003053 (2009).

48. Halbleib, J. M. & Nelson, W. J. Cadherins in development: cell adhesion, sorting, and tissue morphogenesis. *Genes Dev.* **20,** 3199–3214 (2006).

49. Jones, J. C. Characterization of a 125K glycoprotein associated with bovine epithelial desmosomes. *J. Cell Sci.* **89 (Pt 2),** 207–216 (1988).

50. Gumbiner, B., Stevenson, B. & Grimaldi, A. The role of the cell adhesion molecule uvomorulin in the formation and maintenance of the epithelial junctional complex. *J. Cell Biol.* **107,** 1575–1587 (1988).

51. Lewis, J. E., Jensen, P. J. & Wheelock, M. J. Cadherin function is required for human keratinocytes to assemble desmosomes and stratify in response to calcium. *J. Invest. Dermatol.* **102,** 870–877 (1994).

52. Wheelock, M. J. & Jensen, P. J. Regulation of keratinocyte intercellular junction organization and epidermal morphogenesis by E-cadherin. *J. Cell Biol.* **117,** 415–425 (1992).

53. Amagai, M. *et al.* Delayed assembly of desmosomes in keratinocytes with disrupted classic-cadherin-mediated cell adhesion by a dominant negative mutant. *J. Invest. Dermatol.* **104,** 27–32 (1995).

54. Michels, C., Buchta, T., Bloch, W., Krieg, T. & Niessen, C. M. Classical Cadherins Regulate Desmosome Formation. *J Investig Dermatol* **129,** 2072–2075 (2009).

55. Tinkle, C. L., Pasolli, H. A., Stokes, N. & Fuchs, E. New insights into cadherin function in epidermal sheet formation and maintenance of tissue integrity. *Proc. Natl. Acad. Sci. USA* **105,** 15405–15410 (2008).

56. Stepniak, E., Radice, G. L. & Vasioukhin, V. Adhesive and signaling functions of cadherins and catenins in vertebrate development. *Cold Spring Harb. Perspect. Biol.* **1,** a002949 (2009).

57. Kowalczyk, A. P. & Nanes, B. A. Adherens junction turnover: regulating adhesion through cadherin endocytosis, degradation, and recycling. *Subcell. Biochem.* **60,** 197–222 (2012).

58. Li, H., Yen, C.-F. & Sivasankar, S. Fluorescence axial localization with nanometer accuracy and precision. *Nano Lett* **12,** 3731–3735 (2012).

59. Lowndes, M. *et al.* Different roles of cadherins in the assembly and structural integrity of the desmosome complex. *J. Cell Sci.* **127,** 2339–2350 (2014).

60. Butt, H.-J., Cappella, B. & Kappl, M. Force measurements with the atomic force microscope: Technique, interpretation and applications. *Surf. Sci. Rep.* **59,** 1–152 (2005).

61. Hughes, M. L. & Dougan, L. The physics of pulling polyproteins: a review of single molecule force spectroscopy using the AFM to study protein unfolding. *Rep. Prog. Phys.* **79,** 076601 (2016).

62. Manibog, K., Yen, C. F. & Sivasankar, S. *Measuring Force-Induced Dissociation Kinetics of Protein Complexes Using Single-Molecule Atomic Force Microscopy.* **582,** 297–320 (2017).

63. Hutter, J. L. & Bechhoefer, J. Calibration of atomic-force microscope tips. *Rev. Sci. Instrum.* **64,** 1868 (1993).

64. Burnham, N. A. *et al.* Comparison of calibration methods for atomic-force microscopy cantilevers. *Nanotechnology* **14,** 1–6 (2003).

65. Oesterhelt, F., Rief, M. & Gaub, H. E. Single molecule force spectroscopy by AFM indicates helical structure of poly(ethylene-glycol) in water. *New J Phys* **1,** 6–6 (1999).

66. Ray, C., Brown, J. R. & Akhremitchev, B. B. Rupture force analysis and the associated systematic errors in force spectroscopy by AFM. *Langmuir* **23,** 6076–6083 (2007).

67. Bell, G. I. Models for the specific adhesion of cells to cells. *Science (80-.).* **200,** 618–627 (1978).

68. Evans, E. & Ritchie, K. Dynamic strength of molecular adhesion bonds. *Biophys. J.* **72,** 1541–1555 (1997).

CHAPTER 2. RESOLVING DESMOSOMAL CADHERIN INTERACTIONS AT SINGLE MOLECULE LEVEL

2.1 Introduction

The data presented in this chapter were published in Journal of Cell Science in 2014[1]. Single molecule force spectroscopy data described here were collected by Dr. Sabyasachi Rakshit (a former postdoctoral scholar in the lab) and me. All the cell-based assays were carried out by Dr. Molly Lowndes from Prof. James Nelson's lab (Stanford University).

Desmosomal cadherins form the desmosome complex, a vital intercellular adhesive junction that couples to the intermediate filament cytoskeleton. Desmosomes mechanically integrate cells and enable them to resist mechanical stress, maintain robust cell adhesion and tissue morphogenesis [2,3].The importance of desmosome is highlighted by the prominent distribution of desmosomes in tissues that experience mechanical stress such as the heart, skin and hair [3,4]. The desmosomal cadherin subfamily consists of desmogleins (Dsg1–4) and desmocollins (Dsc1–3) that show tissue and differentiation specific expression patterns[5–7]. Their functional essentiality is evident in the wide range of desmosomal diseases that result from disruption of desmosome function[8–12]. For example, the intercalated discs that connect heart muscle cells contain one isoform of each subtype (Dsc2 and Dsg2) [13] and mutations in Dsc2 and Dsg2 cause hereditary diseases such as arrhythmogenic right ventricular cardiomyopathy (ARVC) [9,14,15]. Several of these hereditary mutations have been mapped to the extracellular domain of Dsg2 and Dsc2 [16–18]. Recent studies have found that Dsg2 is a primary receptor used by adenovirus serotypes causing respiratory tract infections. In epithelial cancer cells, adenovirus binding to Dsg2 triggers opening of epithelial junctions which greatly improves the penetration and efficacy of therapeutic agents[19,20]. In the stratified complex epithelia, such as the epidermis, Dsg1/3 and Dsc1/3 are primarily expressed and Dsg4 concentrated in the granular and cornified layers [7]. Autoimmune diseases such as

pemphigus foliaceus and pemphigus vulgaris target extracellular binding of Dsg1 and Dsg3 causing loss of adhesion in the epidermis and mucosal membranes [9,21]. Dsg1 gene cause striate palmoplantar keratoderma [22], an epidermal-thickening disease, whereas mutations in Dsg4 result in defective hair-follicle differentiation [23].

Dsc and Dsg include five extracellular cadherin repeats, each of which form Ig-like globular domains with calcium binding sites in between each pair of consecutive repeats[24]. The cytoplasmic domain of both desmosomal cadherins contain an intracellular anchor (IA) and a cadherin-like sequence (ICS), which is conserved in classical cadherins. The Dsgs have additional unique sequences with unknown functions, including a proline rich linker region (IPL), a repeat unit domain (RUD) and a desmoglein terminal domain (DTD)[25]. Dsc has two differently spliced isoforms type 'a' and the shorter type 'b' with ICS domain truncated [26].

Plakoglobin, an armadillo protein binds to the ICS domain of the desmosomal cadherins and to desmoplakin (DP) [13,27]. DP is an obligate desmosomal protein that couples intermediate filaments to the desmosomal plaque[28–30]. Biochemical and cryo-electron microscopy tomography suggest that DP, through interactions with other desmosome proteins drives clustering and lateral interactions between desmosomal cadherins[31,32].

Both Dsg and Dsc are thought to be involved in extracellular trans interactions between adjacent cells that are important in cell adhesion and tissue morphogenesis [5,33–36]. How Dsc and Dsg combine to form adhesive bonds is unclear, since different binding properties have been assigned to the most ubiquitously expressed isoforms (Dsg2, Dsc2) depending on the assay used [37]. Knock-down of either Dsc2 or Dsg2 expression results in a loss of functional desmosomes[33]. Cell-free studies showed that the EC1-2 domain of Dsc2 can form homophilic bonds and heterophilic bonds with Dsg2, but the EC1-2 domain of Dsg2 does not form homophilic bonds[38]. In contrast, Atomic Force Microscope (AFM) experiments with dimeric Fc fusion proteins indicated that Dsg2 can also form homophilic bonds [39,40]. Cell-based assays in keratinocytes using cross-linking reagents found only homophilic binding of either Dsg2 and

Dsc2 [41]. Thus, the requirement for both Dsg2 and Dsc2 in the structural organization and maintenance of the desmosomal complex remains unclear.

Desmosomal cadherins contain evolutionarily conserved domains with low sequence similarity (~30-40%) to classical cadherins [42].The structure of trans-bound classical cadherins identified a critical tryptophan at position 2 (W2) in the first N-terminal extracellular (EC1) repeat that forms a “strand swap dimer” with the opposing cadherin [43,44]. An alanine substitution (W2A), which inhibits strand swap dimerization, revealed a second configuration termed the X-dimer which involves residues near the EC1-EC2 calcium binding sites, and is thought to be an intermediate that facilitates the formation of the W2 strand-swap dimer [44–46]. The key amino acids involved in strand swapping are conserved in desmosomal cadherins [47–49]. Evidence suggests that desmosomal cadherins interact at their EC1 domains [50–52] while anti-adhesion peptides derived from the sequences of the cell adhesion recognition sites in the EC1 domain block adhesion of both classical and desmosomal cadherins[53,54]. Significantly, homophilic binding of Dsc2 is blocked by mutations in W2, and A80, which contributes to the hydrophobic pocket into which W2 inserts during strand swapping [41], but there is no sequence homology in desmosomal cadherins to residues required for the X-dimer. Thus, the requirement for both Dsg and Dsc in the structural organization and maintenance of the desmosomal complex remains unclear.

To distinguish the roles of Dsc2 and Dsg2, I used single Molecule Force Spectroscopy (SMFS) with wild-type and W2A mutant monomeric Dsg2 and Dsc2; our collaborators used desmosome assembly assay using dual-patterned surfaces containing purified Dsg2, Dsc2 or a combination of Dsc2+Dsg2 and collagen IV; and a cell-based assay to examine the organization and stability of wild-type and W2A mutant Dsg2 and Dsc2 in desmosomes. Our results identified unique roles of Dsc2 and Dsg2 in desmosome organization.

2.2 Results

2.2.1 Desmosomal cadherins have distinct binding properties

To directly address whether Dsc2 and Dsg2 form homophilic and/or heterophilic interactions, I measured their binding using SMFS with an AFM. I used monomeric Dsc2 and Dsg2 fusion proteins, as described previously for E-cadherin [46,55,56], comprising the extracellular domain of Dsc2 or Dsg2 fused at the C-terminal to an Avi tag (A), a TEV-removable (T) His tag (H) (pATH; Figure 2.1A). The purified proteins had expected molecular weights of ~90 kDa, similar to E-cadherin extracellular domain fused to the same tag (Figure 2.1B); a slower migrating protein was detected occasionally and is likely the uncleaved precursor (* in Figure 2.1B).

Purified Dsg2 and Dsc2 monomers were biotinylated and immobilized via PEG linkers to a glass coverslip and an AFM cantilever tip (Figure 2.1C), as described previously for E-cadherin [56–58]. The AFM tip and coverslip were first brought into contact so that opposing cadherins formed adhesive interactions, the tip was then withdrawn from the surface so that force was applied to the adhesive bond. Single molecule interactions were identified from the freely-jointed chain stretching of the polymer tether that anchored the proteins to the surface [1,59] (Figure 2.1D); the contour length of the stretched polymer was used to distinguish specific interactions from non-specific binding. Dsg2 and Dsc2 densities on the AFM tip and coverslip were adjusted to yield binding frequencies in the 5% range (Poisson statistics predicts that more than 95% of the measured events at this unbinding frequency occur due to single molecule unbinding), and the adjusted densities were kept constant for all experimental conditions.

The homophilic binding between (Dsg2:Dsg2 or Dsc2:Dsc2) or heterophilic (Dsg2:Dsc2) interactions was measured in the presence of Ca^{2+} or EGTA, a Ca^{2+} chelator (Figure 2.1E). Non-specific binding rates were measured using identically processed AFM

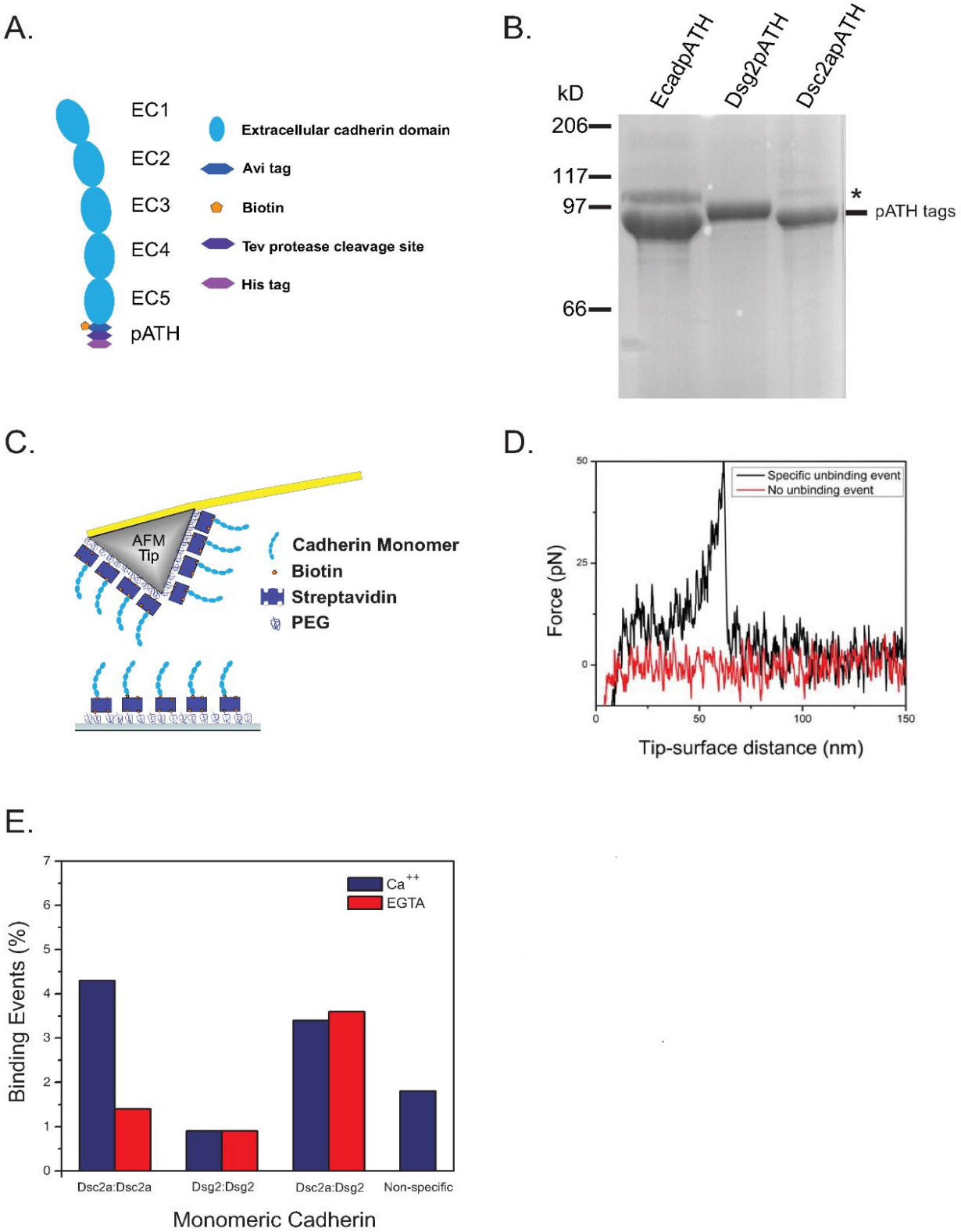

Figure 2.1: Desmosomal cadherins have distinct extracellular trans binding properties.
(A) A schematic of the monomeric desmosomal cadherins fused to tags comprising Avidin,

Tev and His (pATH). (B) Coomassie-blue stained SDS-PAG of purified Dsg2, Dsc2 and Ecad (control) have similar molecular masses (~95 kD); an unprocessed precursor form of the cadherins is present at low levels in the Dsc2 sample (*). (C) Schematic of an AFM cantilever tip and coverslip coated with PEG (5% coverage) and functionalized with monomeric Dsg2 or Dsc2 to measure single molecule interactions. (D) The AFM cantilever tip was lowered and raised thousands of times to measure hundreds of single molecule interactions between protein on the AFM tip and protein on the coverslip, and only events showing a single binding event were used for analysis. (E) Single molecule binding frequency of different combinations of Dsg2 and Dsc2 was plotted as a percentage of all events and compared to non-specific binding (identically functionalized cantilevers lacking the desmosomal cadherins). Addition of the Ca^{2+} chelator EGTA was used to test Ca^{2+} dependence of binding events. Figure adapted from Lowndes et al. J Cell Sci. 2014.

cantilevers and coverslips that were not decorated with Dsg2 or Dsc2. The binding frequency (percentage) showed that the greatest number of unbinding events involved homophilic interactions between Dsc2 (>4%), and that binding was significantly reduced to less than 2% upon addition of EGTA indicating a Ca^{2+} dependent binding mechanism. In contrast, homophilic binding between Dsg2 was less than 1%, which was below that of non-specific binding events (Figure 2.1E). I detected heterophilic binding events between Dsc2 and Dsg2, and the frequency of those binding events was similar in the presence or absence of Ca^{2+}, indicating a Ca^{2+} independent binding mechanism (Figure 2.1E). Since Dsg2 bound to Dsc2 via heterophilic interactions, the lack of homophilic Dsg2 binding is not due to inactivity of Dsg2.

2.2.2 W2 is required for Dsc2 Ca^{2+} dependent homophilic binding not for heterophilic interaction with Dsg2

The amino acid sequence of the extracellular domain of classical and desmosomal cadherins contains a tryptophan at position 2 (W2) in the first extracellular domain (EC1). W2 in classical cadherins is crucial for trans binding between opposing extracellular domains [60,61] because it forms a strand swap dimer between opposing cadherins [43,44]. It has been

suggested that desmosomal cadherins use a similar binding mechanism [49,62]. To test the role of W2, we made alanine substitution mutants in Dsc2 (Dsc2W2A) and in Dsg2 (Dsg2W2A) and were used for SMFS (Figure 2.2).

The W2A mutation resulted in loss of Ca^{2+} dependent Dsc2 homophilic binding measured by SMFS, since the cadherin binding frequency did not change when free Ca^{2+} was chelated by EGTA (Figure 2.2), unlike the wild-type Dsc2 (see Figure 2.1E). However, the frequency of Ca^{2+} independent heterophilic binding between Dsc2W2A and Dsg2W2A (Figure 2.2) was similar to the wild-type protein binding (Figure 2.1E). These results indicate that homophilic Dsc2:Dsc2 binding is Ca^{2+} dependent and requires a strand-swap mechanism involving W2. In contrast, heterophilic binding between Dsc2 and Dsg2 is Ca^{2+} independent and occurs by a W2-independent mechanism. This is in contrast to E-cadherin, in which mutations of both W2 and K14 residues are required to inhibit binding [44,56].

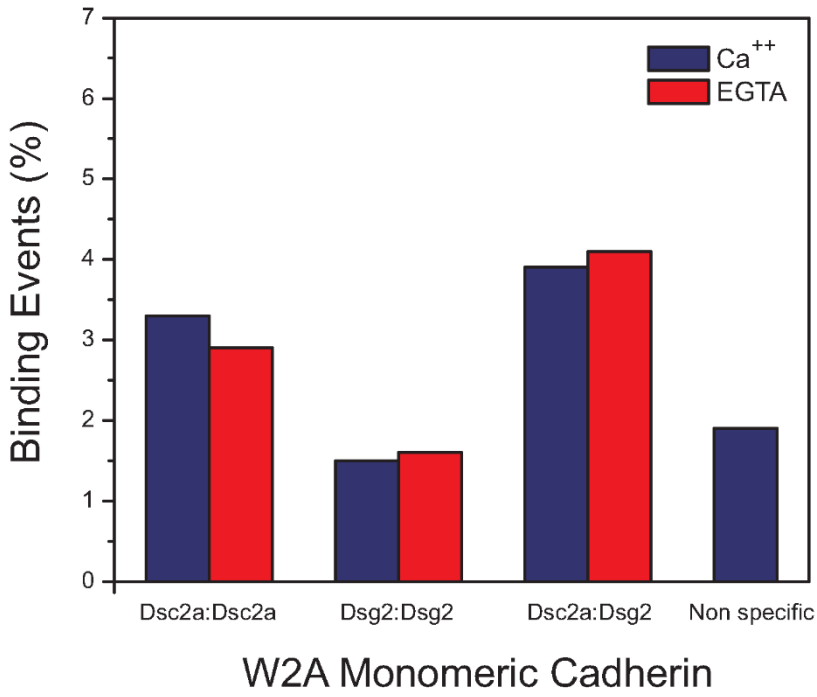

Figure 2.2: W2A substitution in Dsc2 disrupts single molecule trans binding.
SMFS showed low levels of Ca^{2+} independent homophilic binding of Dsg2W2A and Dsc2W2A. Ca^{2+} independent heterophilic binding of Dsg2W2A and Dsc2W2A was comparable to wild type (Figure 2.1E). Figure adapted from Lowndes et al. J Cell Sci. 2014.

2.2.3 Different requirements of desmosomal cadherins for the formation of punctate desmosomal structures

Our collaborators used micro-patterned surfaces of Dsc2 and/or Dsg2, and the extracellular matrix protein collagen IV, adapted from previous study [63] to distinguish roles of Dsg2 and Dsc2 in desmosome adhesion and assembly. This assay uncouples desmosome assembly from other cell adhesion complexes such as E-cadherin. DP distribution on the ventral membrane of the MDCK cells was determined using a Total Internal Reflection Fluorescence (TIRF) Microscopy.

This assay showed cellular DP distribution was restricted over stripes containing Dsg2Fc, Dsc2Fc or Dsg2Fc+Dsc2Fc, and generally excluded from areas over the collagen IV stripe. Significantly, the organization of DP was diffuse over the Dsg2Fc, but more punctate over the Dsc2aFc stripe and Dsg2Fc+Dsc2aFc stripe. These results indicated that Dsc2 is necessary and sufficient to recruit DP into desmosome-like puncta, while Dsg2 is not required on at least one of the opposing surfaces.

2.2.4 W2 is required for Dsc2 recruitment into desmosome puncta not for Dsg2

To identify the importance of W2 in desmosome assembly, our collaborators used Dsg2W2A and Dsc2W2A GFP-tagged mutants transiently expressed in MDCK cells. Their immunofluorescence data showed that Dsg2W2A-GFP was restricted to puncta along cell-cell contacts, similar to wild-type Dsg2-GFP. However, Dsc2W2A-GFP had a linear distribution along the plasma membrane at cell-cell contacts compared to wild-type Dsc2-GFP. This experiment showed that W2 and strand-swap dimers are not required for Dsg2 incorporation into desmosome puncta but required for Dsc2 incorporation into desmosome puncta.

2.3 Discussion

Desmosomes assemble in a Ca^{2+} -dependent manner between opposing cells and are required to maintain the structural integrity of tissues. Dsg2 and Dsc2 are obligate cadherins in desmosomes, and impairment of either Dsc2 or Dsg2 extracellular interactions causes heart defects, and epidermal blistering diseases and syndromes [12,64]. Studies using different in vitro binding and cell-based assays, however, have not identified specific roles for Dsg2 and Dsc2 in desmosome assembly and adhesion. Whether there is specificity in the extracellular binding properties of desmosomal cadherins has been difficult to establish due to the overlapping roles of other cadherins (e.g. E-cadherin) in epithelial cell-cell adhesion, the complexity of proteins in desmosomes and their resistance to dissociation in non-denaturing conditions [62], and the lack of complete crystal structures of the two desmosomal cadherin sub-types. Here, we used reductionist approaches to distinguish roles of Dsc2 and Dsg2 in desmosome assembly, organization and adhesion in the absence of other cell-cell adhesions. Our results indicate that Dsc2 and Dsg2 have distinct binding properties and functions in desmosome organization and adhesion.

SMFS results indicated that Dsc2 forms homophilic interactions in the presence of Ca^{2+}, and heterophilic interactions with Dsg2 independent of Ca^{2+}. In contrast the Dsg2 was involved only in heterotypic binding. Interestingly, other studies using chemical cross-linkers only found homophilic binding by Dsc2 and Dsg2 [62], while bulk biochemical assays indicated heterophilic Dsc2-Dsg2 binding and weak homophilic Dsg2-Dsg2 binding in agreement with our SMFS results [38]. Differences between other SMFS results [39,65] and our SFMS experiments may be due to our strict definition of a single molecule interaction. Significantly, the W2A mutation in Dsc2 inhibited Ca^{2+} -dependent homophilic binding while heterophilic interaction of Dsc2 and Dsg2 was independent of W2.

Our collaborator's work using micro-patterned substrates of purified Dsc2Fc or Dsg2Fc confirmed that Dsc2, but not Dsg2, was necessary and sufficient to induce the recruitment of a desmosome-specific cytoplasmic protein DP into punctate cellular structures. Since MDCK cells express both Dsc2 and Dsg2 [66,67] the exogenous substrate-bound Dsc2 could have initiated the assembly of desmosome puncta by binding either cellular Dsc2, Dsg2 or both on the ventral surface of the cell.

Furthermore, immunofluorescence studies of our collaborators showed that the Dsc2W2A mutant appeared to be excluded from endogenous desmosomes in MDCK cells, inferred from its linear plasma membrane staining compared to endogenous desmosome puncta in the same cells. Since Dsc2 alone was necessary and sufficient to induce desmosome like DP puncta in cells on micro-patterned substrates, we suggest that Dsc2 homophilic binding via a Ca^{2+} and W2 (strand-swap dimer) dependent mechanism is required for desmosome assembly and incorporation of Dsc2 to desmosome.

In contrast, the W2A mutation in Dsg2 didn't affect the co-localization with endogenous desmosome puncta in MDCK cells. These results indicate that Dsg2 incorporation into desmosomes occurs via a Ca^{2+} and W2 (strand swap dimer) independent mechanism that relies on heterophilic interactions and/or cytoplasmic interactions with other proteins in the desmosome. Differences in Ca^{2+} dependency of desmosomal adhesion have been identified in tissue and cell-based studies, and it has been suggested that mature desmosome complexes are in a hyper-adhesive state that is Ca^{2+} independent [68,69]. Our results raise the possibility that such Ca^{2+} independent adhesion might be mediated by heterophilic Dsc2/Dsg2 binding.

In summary, our results have uncovered a specific role for extracellular contacts formed by Dsc2 in the structural organization and function of desmosomes. The assembly of desmosome puncta depends on Ca^{2+} and W2 (strand-swap dimer) dependent homophilic trans-dimerization between Dsc2 proteins on opposing cell surfaces. Dsg2 may be required

for the long-term stability of desmosomes, and perhaps the formation of a Ca^{2+} independent hyperadhesive state. While Dsc2 may have a specific role in adhesion, Dsg2 may have additional roles [70,71]. Thus, differences in the mechanisms of incorporation and function of Dsc and Dsg cadherins may allow a diversification of desmosome functions in cell adhesion, migration and differentiation.

2.4 Materials and Methods

2.4.1 Protein Purification

Monomeric Dsg2 and Dsc2 construct design was similar to described previously [55], where the C-terminal of the extracellular domain was fused to Avi-tag, Tev sequence and His-tag (pATH). Fusion constructs were expressed in HEK293T cells, and proteins were purified from conditioned medium over Ni-NTA agarose beads, and protein was biotinylated using BirA enzyme for surface functionalization (BirA500 kit, Avidity LLC, Aurora, CO, USA).

2.4.2 Single Molecule Force Spectroscopy (SMFS)

AFM cantilevers and glass coverslips were first cleaned with a 25% H_2O_2:75% H_2SO_4 solution and subsequently washed with deionized water, 1M potassium hydroxide solution, deionized water and acetone. The cleaned AFM cantilevers and coverslips were made amine reactive by functionalizing with 2% v/v solution of 3-Aminopropyltriethoxysilane (Sigma-Aldrich, St. Louis, MO, USA) dissolved in acetone. The cantilevers and coverslips were then functionalized with polyethylene glycol spacers (PEG 5000, Laysan Bio, Arab, AL, USA) containing an amine-reactive N-hydroxysuccinimide ester at one end to bind to the surface. A known fraction of PEG presented biotin at the other end and was kept low in order to measure single molecule events; for wild-type and mutant monomers, 5% and 7% of the PEG contained biotin, respectively. The biotinylated surfaces were incubated with 0.1 mg/ml BSA for 12 hours to minimize non-specific surface interactions, and then with 0.1 mg/ml streptavidin for 30

minutes. Biotinylated Dsc2 or Dsg2 monomers were bound to streptavidin on the AFM tip and coverslip surfaces. Following Dsc2 or Dsg2 immobilization, the surfaces were incubated in 10 μM biotin to block free biotin binding sites on streptavidin.

SMFS experiments were performed at different pulling velocities using an Agilent 5500 AFM. Experiments were performed in 10 mM Tris-HCl, pH 7.5, 100 mM NaCl, 10 mM KCl in either 2.5 mM $CaCl_2$ or 2 mM EGTA. Single unbinding force curves were selected and fitted with the Extended freely jointed chain (ExFJC) model [72] as described in the introduction. Spring constants of the AFM cantilevers were measured with the thermal fluctuation method[73].

2.5 References

1. Lowndes, M. *et al.* Different roles of cadherins in the assembly and structural integrity of the desmosome complex. *J. Cell Sci.* **127,** 2339–2350 (2014).
2. Getsios, S., Huen, A. C. & Green, K. J. Working out the strength and flexibility of desmosomes. *Nat. Rev. Mol. Cell Biol.* **5,** 271–281 (2004).
3. Kowalczyk, A. P. & Green, K. J. Structure, function, and regulation of desmosomes. *Prog Mol Biol Transl Sci* **116,** 95–118 (2013).
4. Holthöfer, B., Windoffer, R., Troyanovsky, S. & Leube, R. E. in **264,** 65–163 (Elsevier, 2007).
5. Dusek, R. L., Godsel, L. M. & Green, K. J. Discriminating roles of desmosomal cadherins: beyond desmosomal adhesion. *J. Dermatol. Sci.* **45,** 7–21 (2007).
6. Hatzfeld, M., Keil, R. & Magin, T. M. Desmosomes and intermediate filaments: their consequences for tissue mechanics. *Cold Spring Harb. Perspect. Biol.* **9,** (2017).
7. Green, K. J. & Simpson, C. L. Desmosomes: new perspectives on a classic. *J. Invest. Dermatol.* **127,** 2499–2515 (2007).
8. Broussard, J. A., Getsios, S. & Green, K. J. Desmosome regulation and signaling in disease. *Cell Tissue Res.* **360,** 501–512 (2015).
9. Amagai, M. Autoimmune and infectious skin diseases that target desmogleins. *Proc. Jpn. Acad. Ser. B. Phys. Biol. Sci.* **86,** 524–537 (2010).
10. Samuelov, L. & Sprecher, E. Inherited desmosomal disorders. *Cell Tissue Res.* **360,** 457–475 (2015).

11. Waschke, J. The desmosome and pemphigus. *Histochem. Cell Biol.* **130,** 21–54 (2008).

12. Thomason, H. A., Scothern, A., McHarg, S. & Garrod, D. R. Desmosomes: adhesive strength and signalling in health and disease. *Biochem. J.* **429,** 419–433 (2010).

13. Delva, E., Tucker, D. K. & Kowalczyk, A. P. The desmosome. *Cold Spring Harb. Perspect. Biol.* **1,** a002543 (2009).

14. Dieding, M. *et al.* Arrhythmogenic cardiomyopathy related DSG2 mutations affect desmosomal cadherin binding kinetics. *Sci. Rep.* **7,** 13791 (2017).

15. Syrris, P. *et al.* Arrhythmogenic right ventricular dysplasia/cardiomyopathy associated with mutations in the desmosomal gene desmocollin-2. *Am. J. Hum. Genet.* **79,** 978–984 (2006).

16. Gehmlich, K. *et al.* Mechanistic insights into arrhythmogenic right ventricular cardiomyopathy caused by desmocollin-2 mutations. *Cardiovasc. Res.* **90,** 77–87 (2011).

17. Gehmlich, K. *et al.* Molecular changes in the heart of a severe case of arrhythmogenic right ventricular cardiomyopathy caused by a desmoglein-2 null allele. *Cardiovasc Pathol* **21,** 275–282 (2012).

18. Schlipp, A. *et al.* Desmoglein-2 interaction is crucial for cardiomyocyte cohesion and function. *Cardiovasc. Res.* **104,** 245–257 (2014).

19. Wang, H. *et al.* Structural and functional studies on the interaction of adenovirus fiber knobs and desmoglein 2. *J. Virol.* **87,** 11346–11362 (2013).

20. Wang, H. *et al.* Desmoglein 2 is a receptor for adenovirus serotypes 3, 7, 11 and 14. *Nat. Med.* **17,** 96–104 (2011).

21. Amagai, M. & Stanley, J. R. Desmoglein as a target in skin disease and beyond. *J. Invest. Dermatol.* **132,** 776–784 (2012).

22. Rickman, L. *et al.* N-terminal deletion in a desmosomal cadherin causes the autosomal dominant skin disease striate palmoplantar keratoderma. *Hum. Mol. Genet.* **8,** 971–976 (1999).

23. Kljuic, A. *et al.* Desmoglein 4 in hair follicle differentiation and epidermal adhesion: evidence from inherited hypotrichosis and acquired pemphigus vulgaris. *Cell* **113,** 249–260 (2003).

24. Brasch, J., Harrison, O. J., Honig, B. & Shapiro, L. Thinking outside the cell: how cadherins drive adhesion. *Trends Cell Biol.* **22,** 299–310 (2012).

25. Koch, P. J. *et al.* Identification of desmoglein, a constitutive desmosomal glycoprotein, as a member of the cadherin family of cell adhesion molecules. *Eur. J. Cell Biol.* **53,** 1–12 (1990).

26. Saito, M., Tucker, D. K., Kohlhorst, D., Niessen, C. M. & Kowalczyk, A. P. Classical and desmosomal cadherins at a glance. *J. Cell Sci.* **125,** 2547–2552 (2012).

27. Peifer, M., McCrea, P. D., Green, K. J., Wieschaus, E. & Gumbiner, B. M. The vertebrate adhesive junction proteins beta-catenin and plakoglobin and the Drosophila segment polarity gene armadillo form a multigene family with similar properties. *J. Cell Biol.* **118,** 681–691 (1992).

28. Bornslaeger, E. A., Corcoran, C. M., Stappenbeck, T. S. & Green, K. J. Breaking the connection: displacement of the desmosomal plaque protein desmoplakin from cell-cell interfaces disrupts anchorage of intermediate filament bundles and alters intercellular junction assembly. *J. Cell Biol.* **134,** 985–1001 (1996).

29. Gallicano, G. I. *et al.* Desmoplakin is required early in development for assembly of desmosomes and cytoskeletal linkage. *J. Cell Biol.* **143,** 2009–2022 (1998).

30. Kowalczyk, A. P. *et al.* The amino-terminal domain of desmoplakin binds to plakoglobin and clusters desmosomal cadherin-plakoglobin complexes. *J. Cell Biol.* **139,** 773–784 (1997).

31. Kowalczyk, A. P. *et al.* The head domain of plakophilin-1 binds to desmoplakin and enhances its recruitment to desmosomes. Implications for cutaneous disease. *J. Biol. Chem.* **274,** 18145–18148 (1999).

32. Al-Amoudi, A. *et al.* The three-dimensional molecular structure of the desmosomal plaque. *Proc. Natl. Acad. Sci. USA* **108,** 6480–6485 (2011).

33. Roberts, G. A. *et al.* Antisense expression of a desmocollin gene in MDCK cells alters desmosome plaque assembly but does not affect desmoglein expression. *Eur. J. Cell Biol.* **76,** 192–203 (1998).

34. Chitaev, N. A. & Troyanovsky, S. M. Direct Ca2+-dependent heterophilic interaction between desmosomal cadherins, desmoglein and desmocollin, contributes to cell-cell adhesion. *J. Cell Biol.* **138,** 193–201 (1997).

35. Marcozzi, C., Burdett, I. D., Buxton, R. S. & Magee, A. I. Coexpression of both types of desmosomal cadherin and plakoglobin confers strong intercellular adhesion. *J. Cell Sci.* **111 (Pt 4),** 495–509 (1998).

36. Runswick, S. K., O'Hare, M. J., Jones, L., Streuli, C. H. & Garrod, D. R. Desmosomal adhesion regulates epithelial morphogenesis and cell positioning. *Nat. Cell Biol.* **3,** 823–830 (2001).

37. Waschke, J. The desmosome and pemphigus. *Histochem. Cell Biol.* **130,** 21–54 (2008).

38. Syed, S.-H. *et al.* Molecular interactions between desmosomal cadherins. *Biochem. J.* **362,** 317–327 (2002).

39. Schlegel, N. *et al.* Desmoglein 2-mediated adhesion is required for intestinal epithelial barrier integrity. *Am. J. Physiol. Gastrointest. Liver Physiol.* **298,** G774–83 (2010).

40. Hartlieb, E. *et al.* Desmoglein 2 is less important than desmoglein 3 for keratinocyte cohesion. *PLoS One* **8,** e53739 (2013).

41. Nie, Z., Merritt, A., Rouhi-Parkouhi, M., Tabernero, L. & Garrod, D. Membrane-impermeable cross-linking provides evidence for homophilic, isoform-specific binding of desmosomal cadherins in epithelial cells. *J. Biol. Chem.* **286,** 2143–2154 (2011).

42. Patel, S. D., Chen, C. P., Bahna, F., Honig, B. & Shapiro, L. Cadherin-mediated cell-cell adhesion: sticking together as a family. *Curr. Opin. Struct. Biol.* **13,** 690–698 (2003).

43. Boggon, T. J. *et al.* C-cadherin ectodomain structure and implications for cell adhesion mechanisms. *Science (80-.).* **296,** 1308–1313 (2002).

44. Harrison, O. J. *et al.* Two-step adhesive binding by classical cadherins. *Nat. Struct. Mol. Biol.* **17,** 348–357 (2010).

45. Ciatto, C. *et al.* T-cadherin structures reveal a novel adhesive binding mechanism. *Nat. Struct. Mol. Biol.* **17,** 339–347 (2010).

46. Sivasankar, S., Zhang, Y., Nelson, W. J. & Chu, S. Characterizing the initial encounter complex in cadherin adhesion. *Structure* **17,** 1075–1081 (2009).

47. Nollet, F., Kools, P. & van Roy, F. Phylogenetic analysis of the cadherin superfamily allows identification of six major subfamilies besides several solitary members. *J. Mol. Biol.* **299,** 551–572 (2000).

48. Vendome, J. *et al.* Molecular design principles underlying β-strand swapping in the adhesive dimerization of cadherins. *Nat. Struct. Mol. Biol.* **18,** 693–700 (2011).

49. Posy, S., Shapiro, L. & Honig, B. Sequence and structural determinants of strand swapping in cadherin domains: do all cadherins bind through the same adhesive interface? *J. Mol. Biol.* **378,** 954–968 (2008).

50. in *Encyclopedia of Biophysics* (ed. Roberts, G. C. K.) 392–392 (Springer Berlin Heidelberg, 2013). doi:10.1007/978-3-642-16712-6_100194

51. Al-Amoudi, A., Díez, D. C., Betts, M. J. & Frangakis, A. S. The molecular architecture of cadherins in native epidermal desmosomes. *Nature* **450,** 832–837 (2007).

52. Shimizu, A. *et al.* In vivo ultrastructural localization of the desmoglein 3 adhesive interface to the desmosome mid-line. *J. Invest. Dermatol.* **124,** 984–989 (2005).

53. Runswick, S. K., O'Hare, M. J., Jones, L., Streuli, C. H. & Garrod, D. R. Desmosomal adhesion regulates epithelial morphogenesis and cell positioning. *Nat. Cell Biol.* **3,** 823–830 (2001).

54. Tselepis, C., Chidgey, M., North, A. & Garrod, D. Desmosomal adhesion inhibits invasive behavior. *Proc. Natl. Acad. Sci. USA* **95,** 8064–8069 (1998).

55. Zhang, Y., Sivasankar, S., Nelson, W. J. & Chu, S. Resolving cadherin interactions and binding cooperativity at the single-molecule level. *Proc. Natl. Acad. Sci. USA* **106,** 109–114 (2009).

56. Rakshit, S., Zhang, Y., Manibog, K., Shafraz, O. & Sivasankar, S. Ideal, catch, and slip bonds in cadherin adhesion. *Proc. Natl. Acad. Sci. USA* **109,** 18815–18820 (2012).

57. Manibog, K., Li, H., Rakshit, S. & Sivasankar, S. Resolving the molecular mechanism of cadherin catch bond formation. *Nat Commun* **5,** 3941 (2014).

58. Manibog, K. *et al.* Molecular determinants of cadherin ideal bond formation: Conformation-dependent unbinding on a multidimensional landscape. *Proc. Natl. Acad. Sci. USA* **113,** E5711–20 (2016).

59. Yen, C.-F., Harischandra, D. S., Kanthasamy, A. & Sivasankar, S. Copper-induced structural conversion templates prion protein oligomerization and neurotoxicity. *Sci. Adv.* **2,** e1600014 (2016).

60. Shapiro, L. *et al.* Structural basis of cell-cell adhesion by cadherins. *Nature* **374,** 327–337 (1995).

61. Hong, S., Troyanovsky, R. B. & Troyanovsky, S. M. Cadherin exits the junction by switching its adhesive bond. *J. Cell Biol.* **192,** 1073–1083 (2011).

62. Nie, Z., Merritt, A., Rouhi-Parkouhi, M., Tabernero, L. & Garrod, D. Membrane-impermeable cross-linking provides evidence for homophilic, isoform-specific binding of desmosomal cadherins in epithelial cells. *J. Biol. Chem.* **286,** 2143–2154 (2011).

63. Borghi, N., Lowndes, M., Maruthamuthu, V., Gardel, M. L. & Nelson, W. J. Regulation of cell motile behavior by crosstalk between cadherin- and integrin-mediated adhesions. *Proc. Natl. Acad. Sci. USA* **107,** 13324–13329 (2010).

64. Al-Jassar, C., Bikker, H., Overduin, M. & Chidgey, M. Mechanistic basis of desmosome-targeted diseases. *J. Mol. Biol.* **425,** 4006–4022 (2013).

65. Hartlieb, E. *et al.* Desmoglein 2 is less important than desmoglein 3 for keratinocyte cohesion. *PLoS One* **8,** e53739 (2013).

66. Pasdar, M. & Nelson, W. J. Regulation of desmosome assembly in epithelial cells: kinetics of synthesis, transport, and stabilization of desmoglein I, a major protein of the membrane core domain. *J. Cell Biol.* **109,** 163–177 (1989).

67. Pasdar, M., Krzeminski, K. A. & Nelson, W. J. Regulation of desmosome assembly in MDCK epithelial cells: coordination of membrane core and cytoplasmic plaque domain assembly at the plasma membrane. *J. Cell Biol.* **113,** 645–655 (1991).

68. Garrod, D. R., Berika, M. Y., Bardsley, W. F., Holmes, D. & Tabernero, L. Hyper-adhesion in desmosomes: its regulation in wound healing and possible relationship to cadherin crystal structure. *J. Cell Sci.* **118,** 5743–5754 (2005).

69. Garrod, D. & Tabernero, L. Hyper-adhesion: a unique property of desmosomes. *Cell Commun. Adhes.* **21,** 249–256 (2014).

70. Brennan, D. & Mahoney, M. G. Increased expression of Dsg2 in malignant skin carcinomas: A tissue-microarray based study. *Cell Adh Migr* **3,** 148–154 (2009).

71. Brennan, D. *et al.* Suprabasal Dsg2 expression in transgenic mouse skin confers a hyperproliferative and apoptosis-resistant phenotype to keratinocytes. *J. Cell Sci.* **120,** 758–771 (2007).

72. Oesterhelt, F., Rief, M. & Gaub, H. E. Single molecule force spectroscopy by AFM indicates helical structure of poly(ethylene-glycol) in water. *New J Phys* **1,** 6–6 (1999).

73. Hutter, J. L. & Bechhoefer, J. Calibration of atomic-force microscope tips. *Rev. Sci. Instrum.* **64,** 1868 (1993).

CHAPTER 3. E-CADHERIN BINDS TO DESMOGLEIN TO FACILITATE DESMOSOME ASSEMBLY

Omer Shafraz, Matthias Rübsam, Sara N. Stahley, Amber Caldara, Andrew P. Kowalczyk, Carien M. Niessen, Sanjeevi Sivasankar

This chapter is a manuscript submitted to eLife. The single molecule force AFM force measurements were done by me. I identified an important amino acid (Leu 175) in Ecad that is essential to bring in Dsg2 to desmosome. Our collaborators Dr. Stahley and Ms. Caldara from Prof. Kowalczyk's lab (Emory University) used SIM to show that Ecad is present in early desmosome and it is excluded as desmosome matures. Our collaborators Dr. Rübsam and Prof. Niessen (University of Cologne) used confocal microscopy to show that desmosome assembly is initiated at sites of Ecad trans homodimerization and that Ecad-L175 is required for efficient Dsg2 and DP recruitment to sites of early intercellular contact formation.

3.1 Abstract

Desmosomes are adhesive junctions composed of desmosomal cadherins, desmocollin (Dsc) and desmoglein (Dsg). Previous studies demonstrate that E-cadherin (Ecad) facilitates desmosome assembly via unknown mechanisms. Here we combine AFM, super resolution microscopy and structure/function analysis to resolve the roles of Ecad and isoform 2 of Dsc and Dsg in desmosome assembly. AFM force measurements reveal that Ecad interacts with Dsg2 via a conserved Leu 175 on the Ecad *cis* binding interface. Using super resolution imaging, we demonstrate that while Ecad is present in nascent desmosomes, it is excluded as desmosomes mature. Finally, confocal imaging reveals that desmosome assembly is initiated at sites of Ecad *trans* homodimerization and that Ecad-L175 is required for efficient Dsg2 and desmoplakin recruitment to sites of early intercellular contact formation. Our data indicates that Ecad *trans* interactions at nascent cell-cell contacts initiate the recruitment of Dsg through direct *cis* interactions with Ecad which facilitates desmosome assembly.

3.2 Introduction

The formation, organization and maintenance of complex tissue structures are mediated by the cadherin superfamily of cell-cell adhesion proteins, a large protein group composed of four major subfamilies: classical cadherins, desmosomal cadherins, protocadherins and atypical cadherins[1]. Of these proteins, desmosomal cadherins and classical cadherins are essential for the maintenance of tissue integrity [2]. While classical cadherins mediate cell-cell adhesion in all soft tissue and play critical roles in tissue morphogenesis, desmosomal cadherins mediate robust cell-cell adhesion in tissues like the epidermis and heart that are exposed to significant levels of mechanical stress[3]. There are two types of desmosomal cadherins: desmoglein (Dsg) and desmocollin (Dsc), which are organized into four Dsg isoforms (Dsg1-4) and three Dsc isoforms (Dsc1-3)[4]. Of these isoforms, Dsg2 and Dsc2 are widely expressed in the epithelia and are also found in non-epithelial cells such as in the myocardium of the heart and lymph node follicles [4]. Loss of Dsg2 is embryonically lethal [5] while mutations in Dsg2 [6] and Dsc2 [7] cause arrhythmogenic right ventricular cardiomyopathy (ARVC), a hereditary heart disease. In contrast, isoforms 1 and 3 are restricted to complex epithelial tissues [8] and their loss of function leads to epidermal fragility, such as in the autoimmune blistering disease pemphigus [9].

Dsc and Dsg associate with anchoring and signaling proteins to form robust intercellular junctions called desmosomes. Several studies have shown that the classical cadherin, E-cadherin (Ecad), promotes desmosome assembly. Immuno-electron micrographs demonstrate that Ecad localizes to the intercellular region of the bovine tongue epithelial desmosomes[10]. Blocking Ecad adhesion with antibodies delay desmosome formation in MDCK cells[11] and in human keratinocytes[12,13]. Desmosome formation in keratinocytes requires junctional initiation by the classical cadherins, Ecad or P-cadherin (Pcad)[14,15]. Similarly, Ecad and Pcad deficient mice show defective desmosome assembly[16]. However,

the precise molecular mechanisms by which classical cadherins promote desmosome formation are unknown.

To resolve the mechanistic role of Ecad in desmosome assembly, we characterized the interactions of Ecad, Dsg2 and Dsc2 in different stages of desmosome formation using an integrated structure/function analysis that combined single molecule force measurements of wild type (WT) and mutant cadherins with an atomic force microscope (AFM), super resolution imaging of desmosomes in human keratinocytes and confocal fluorescence microscopy of Ecad-knockout, Pcad-knockdown mouse keratinocytes (E^{KO}/P^{KD}), transfected with WT and mutant cadherins. The data identify a novel Ca^{2+}- independent direct interaction between Ecad and Dsg2 that is mediated by a conserved Leu 175 on the Ecad *cis* binding interface. The data shows that desmosome assembly is initiated in two stages: a first stage that requires stable Ecad *trans*-homodimerization and a second stage characterized by the direct heterophilic binding between Ecad and Dsg2 that facilitates further desmosome assembly. The interactions between Ecad and Dsg2 are short-lived and as desmosomes mature, Dsg2 dissociates from Ecad and forms stable bonds with Dsc2 to mediate robust adhesion.

3.3 Results

3.3.1 Ecad interacts with Dsg2 to form a Ca^{2+}-independent heterodimer

We identified the binding partners for recombinant Dsc2, Dsg2 and Ecad using single molecule AFM force measurements. The complete extracellular region of Dsc2, Dsg2 and Ecad were expressed in mammalian cells and biotinylated at their C-terminus using a biotin ligase enzyme (Methods). Identical concentrations of biotinylated cadherins were immobilized on AFM tips and glass coverslip (CS) substrates that were functionalized with poly ethylene

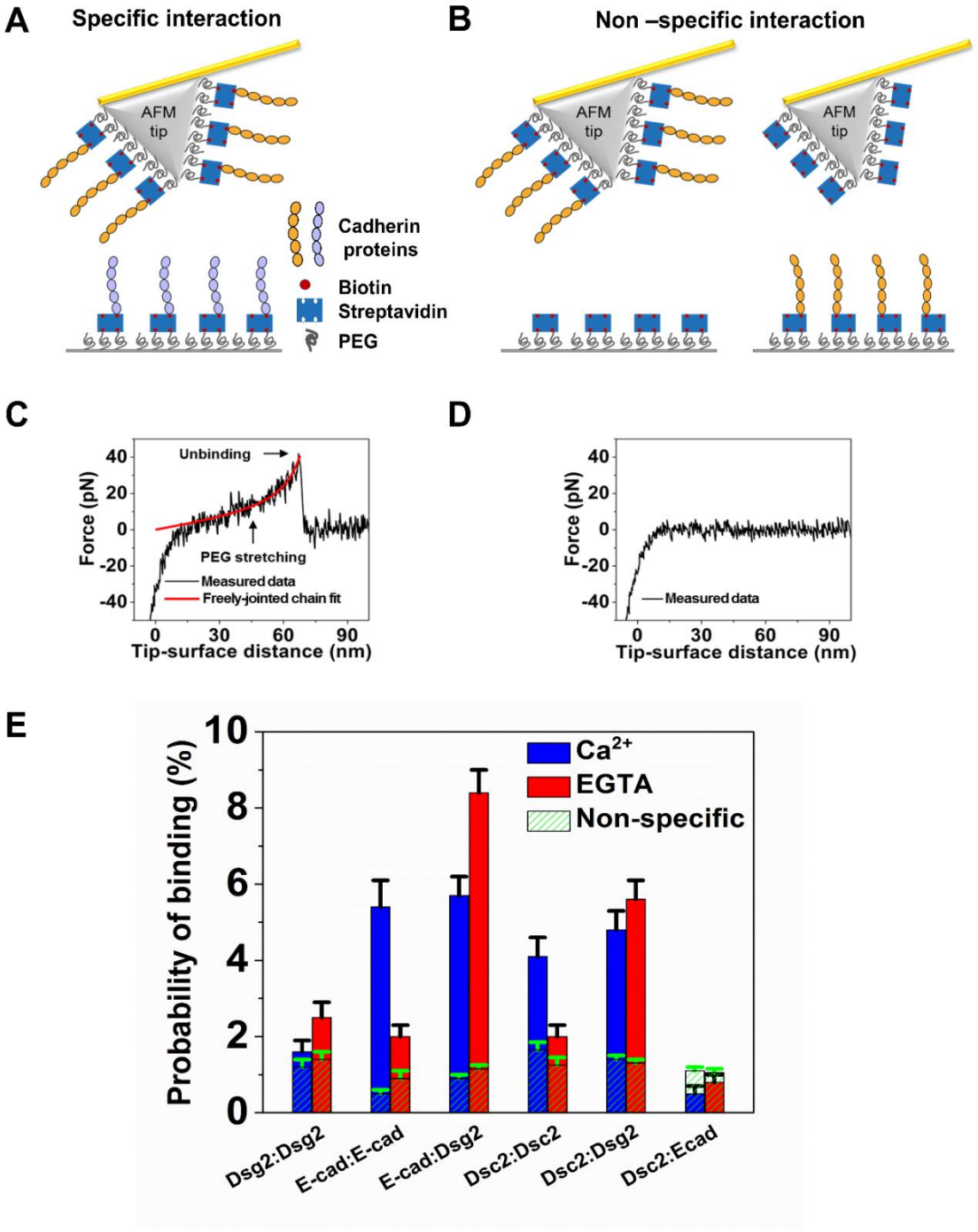

Figure 3.1: Ecad interacts with Dsg2 to form Ca^{2+}-independent dimers: (A) Schematic of specific interaction experiment. The AFM tip and substrate were functionalized with PEG linkers some of which were decorated with streptavidins. Biotinylated cadherin proteins

were attached to streptavidin. (B) Schematic of nonspecific interaction experiment. The probability of interactions between the AFM tip functionalized with biotinylated cadherin proteins and the substrate lacking cadherins *(left)* and the binding probability of a bare AFM cantilever and a substrate decorated with cadherins *(right)* was measured. Example force versus tip-surface distance traces showing (C) a single unbinding event with signature PEG stretching and (D) no interaction. (E) Specific binding probabilities for different combination of cadherins on the tip and substrate measured in Ca^{2+} (blue) and in EGTA (red), a Ca^{2+} chelator. Non-specific binding levels (hatched green) were determined from the average of measured binding probabilities between a cadherin functionalized AFM tip and a bare surface and between a bare AFM tip and surface functionalized with biotinylated cadherin proteins. Dsg2/Dsg2 data was from a total of 1666 (Ca^{2+}) and 1849 (EGTA) measurements; Ecad/Ecad data was from a total of 1052 (Ca^{2+}) and 2150 (EGTA) measurements; Ecad/Dsg2 data was from a total of 2215 (Ca^{2+}) and 2051 (EGTA) measurements; Dsc2/Dsc2 data was from a total of 1658 (Ca^{2+}) and 2025 (EGTA) measurements; Dsc2/Dsg2 data was from a total of 1850 (Ca^{2+}) and 2025 (EGTA) measurements; Dsc2/Ecad data was from a total of 2122 (Ca^{2+}) and 2098 (EGTA) measurements. Error bars are s.e. calculated using bootstrap with replacement.

glycol (PEG) tethers and decorated with streptavidin protein (Figure 3.1 A & 3.1 B), (Methods) [17-21]. Under similar experimental conditions, cadherin surface density was previously determined to be 65 ± 18 cadherins per μm^2, which corresponds to an average distance of 124 nm between neighboring cadherins [21]. Since the separation between neighboring cadherins is an order of magnitude larger than the radius of curvature of the AFM tip, the measured unbinding events correspond to the interaction of only a single cadherin immobilized on the surface and the AFM tip respectively. At the start of the experiment, the AFM cantilever and substrate were brought into contact to allow opposing cadherins to interact. The tip was then withdrawn from the substrate and the force required to rupture the adhesive complex was measured. Interaction of opposing cadherins resulted in unbinding events characterized by non-linear stretching of the PEG tethers (Figure 3.1C); PEG stretching served as a molecular fingerprint for single molecule unbinding since its extension under load has been extensively characterized [22]. If the cadherins did not interact, no unbinding forces were measured (Figure 3.1D).

To determine the adhesive properties of different cadherins, we measured the binding probabilities of various combinations of Dsg2, Dsc2 and Ecad in the presence of Ca^{2+} or in the presence of EGTA, a Ca^{2+} chelating agent. We characterized the levels of nonspecific interactions in every experiment by measuring both the binding probability of a cadherin functionalized AFM cantilever and a bare substrate lacking cadherin and also the binding probability of a bare AFM cantilever and a cadherin-functionalized substrate (Figure 3.1 B); nonspecific binding probabilities (shown as green hatched bars in Figure 3.1 E) are the average of both these sets of measurements. In agreement with our previous results[17], the probability of homophilic Dsg2 interaction in either the presence (1.6 ± 0.3%) or absence (2.5 ± 0.4%) of Ca^{2+} was comparable to nonspecific adhesion (1.2 ± 0.2% in Ca^{2+} and 1.4 ± 0.2% in EGTA). In contrast, Dsc2/Dsc2 showed a Ca^{2+}-dependent homophilic interaction[17], with a binding probability of 4.1 ± 0.5% in Ca^{2+} and 2.0 ± 0.3% in EGTA (corresponding nonspecific binding was 1.6 ± 0.2% and 1.3 ± 0.2% in Ca^{2+} and EGTA, respectively). Heterophilic interactions between Dsc2 (on AFM tip) and Dsg2 (on CS) were Ca^{2+}-independent [17], with binding probabilities of 4.8 ± 0.5% in Ca^{2+} and 5.6 ± 0.5% in EGTA (nonspecific binding levels were 1.4 ± 0.1% and 1.3± 0.1% in Ca^{2+} and EGTA, respectively). As expected, Ecad also showed a Ca^{2+}-dependent homophilic interaction with a binding probability of 5.4 ± 0.7% in Ca^{2+} and 2.0 ± 0.3% in EGTA (corresponding nonspecific binding was 0.5 ± 0.1% in Ca^{2+} and 0.9 ± 0.3% in EGTA) (Figure 3.1E).

Surprisingly, we also measured Ca^{2+}-independent heterophilic interactions between Dsg2 (on CS) and Ecad (on AFM tip) with binding probabilities of 5.7 ± 0.5% and 8.4 ± 0.6% in the presence of Ca^{2+} and EGTA respectively (nonspecific binding: 0.9 ± 0.1% in Ca^{2+} and 1.1 ± 0.1% in EGTA). In contrast, Dsc2 on AFM tip and Ecad on the CS did not show any heterophilic binding either in Ca^{2+} or in EGTA; while a binding probability of 0.5 ± 0.2%, comparable to nonspecific adhesion of 1.1 ± 0.1%, was measured in Ca^{2+}, the binding

frequency of Dsc2/Ecad interactions in EGTA was 0.8 ± 0.2% similar to nonspecific binding of 1.1 ± 0.1%. Our binding probability measurements thus demonstrate that Dsg2 and Ecad form a Ca^{2+}-independent heterophilic dimer while Dsc2 does not bind heterophilically to Ecad.

3.3.2 Ecad/Dsg2 and Dsc2/Dsc2 dimers have lower lifetimes than Dsc2/Dsg2 dimers

Next, we compared the dissociation rates for Dsc2/Dsc2, Dsc2/Dsg2 and Ecad/Dsg2 dimers, in the presence of Ca^{2+}, using single molecule dynamic force spectroscopy (DFS). The cadherins were immobilized on the AFM tip and substrate as described above and the surface density of the protein was empirically adjusted such that the binding probability was ~6%. Under these conditions, Poisson statistics predicts that more than 97% of measured events are from the rupture of single bonds. The single molecule unbinding events, which were characterized by the non-linear stretching of the PEG tethers (Figure 3.1C), were fit to an extended freely-jointed chain model [22] using a total least squares fitting protocol. Specific unbinding events were unambiguously identified since they occurred at a distance corresponding to the contour length of two PEG tethers; only specific unbinding events were used in further analysis (see Methods). The measurements were repeated several thousand times at 6 different rates of application of force (loading rates) and at different positions of the substrate.

The most probable unbinding force at the different loading rates were fit to the Bell-Evans model [23,24] to measure the intrinsic off-rate under zero force, k_{off} and the width of energy barrier that inhibit protein dissociation, x_β (Figure 3.2 A, B, C). We used cluster analysis to group the single molecule unbinding events for fitting [25]. We have previously shown that a K-means clustering algorithm greatly improves the estimation of kinetic parameters in DFS [25]. This analysis showed that the off-rate of Dsc2/Dsc2 dimers (Figure 3.2 A) and Dsg2/Ecad dimers (Figure 3.2 C) were comparable with a k^0_{off} of 1.26 s^{-1} and 1.24 s^{-1} respectively. In

contrast, the lifetime of the Dsc2/Dsg2 dimer (Figure 3.2 B) was longer by an order of magnitude with a smaller k^0_{off} of 0.20 s^{-1}, demonstrating that the Dsg2/Dsc2 dimer was ~10x more stable than either the Dsc2/Dsc2 or the Dsg2/Ecad. These measurements suggest that, upon dissociation of Dsg2/Ecad and Dsc2/Dsc2 complexes, the free Dsg2 and Dsc2 would preferentially bind. In agreement with our data, recent solution binding affinity measurements

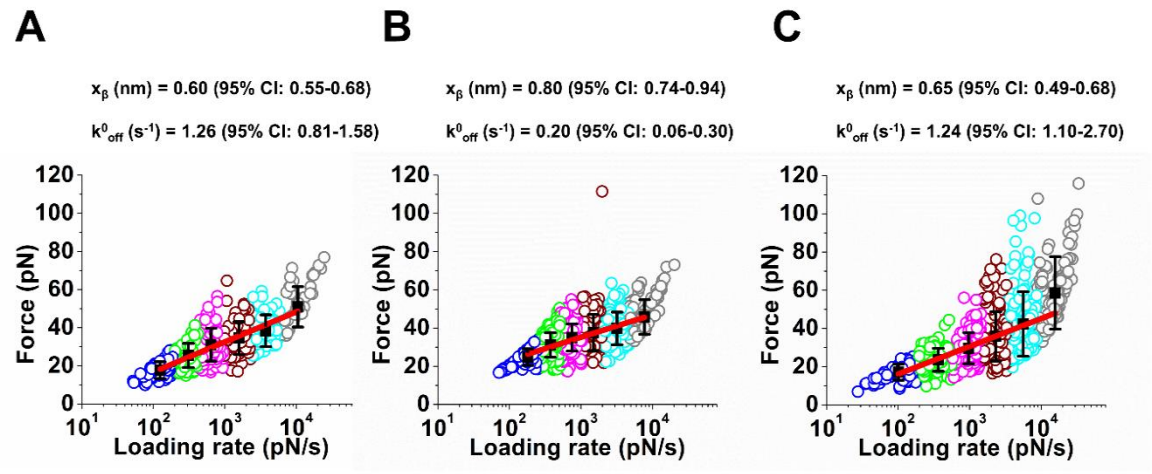

Figure 3.2: Lifetimes of the Ecad/Dsg2 dimer and the Dsc2/Dsc2 dimer are shorter than the lifetime of the Dsg2/Dsc2 complex: Loading rates of the rupture events measured in Ca^{2+} at six different pulling velocities were grouped using K-means clustering method. Each clustered loading rate is shown by a different color, with each circle represent a single rupture event. The mean force and mean loading rates (black filled squares) for the groups were fit to Bell-Evans model (red line) using a nonlinear least-squares fitting with bisquare weights. Fits yielded the intrinsic off-rate (k_{off}^0) and the width of the transition energy barrier (x_β). Error bars in force correspond to standard deviation. 95% confidence interval (CI) was calculated using bootstrap with replacement. Analysis shown for (A) Dsc2/Dsc2 (B) Dsc2/Dsg2 and (C) Ecad/Dsg2. The data shown in panels A, B & C correspond to 415 events, 988 events, and 725 events respectively.

of desmosomal cadherins have shown heterophilic interactions are orders of magnitude stronger than homophilic binding [26].

3.3.3 Ecad is present in nascent desmosomes but not in mature desmosomes

Next, we used SIM to test for the presence of Ecad at different stages of desmosome assembly in human keratinocytes. The keratinocytes were first cultured in a medium containing a low concentration of Ca^{2+} ions not conducive for desmosome formation (100 µM Ca^{2+}) and the Ca^{2+} concentration was then increased to trigger desmosome assembly (550 µM Ca^{2+}), (Methods). At three time points following the Ca^{2+} switch (1 hr, 3 hr and 18 hr), keratinocytes were fixed and immunostained for Dsg2, Ecad and Desmoplakin (DP), a protein that links desmosomal proteins to the intermediate filament cytoskeleton. Since DP is an obligate desmosomal protein, its distribution allowed us to identify individual desmosomes on the keratinocyte surface with desmosomal junctions defined by regions of parallel DP 'railroad tracks' [27,28] (Figure 3.3 A).

Comparison of relative Dsg2 and Ecad levels contained within the DP railroad tracks demonstrated that Ecad levels were high in nascent desmosomes but decreased as the desmosomes matured. Compared to Ecad levels in nascent desmosomes, the intensity of fluorescently labeled Ecad decreased by 50% in mature desmosomes (Figure 3.3 B). In contrast, the relative levels of Dsg2 stayed constant at all time points (Figure 3.3 B). Line scan analysis along cell borders highlight cadherin localization relative to desmosomes as defined by DP 'railroad tracks', confirming Ecad presence in nascent desmosomes and exclusion as desmosomes mature (Figure 3.3 C). In contrast, Dsg2 remained well localized within DP railroad tracks at all time points (Figure 3.3 C). Overall, these data indicate that Ecad is present in nascent desmosomes but becomes excluded as desmosomes mature.

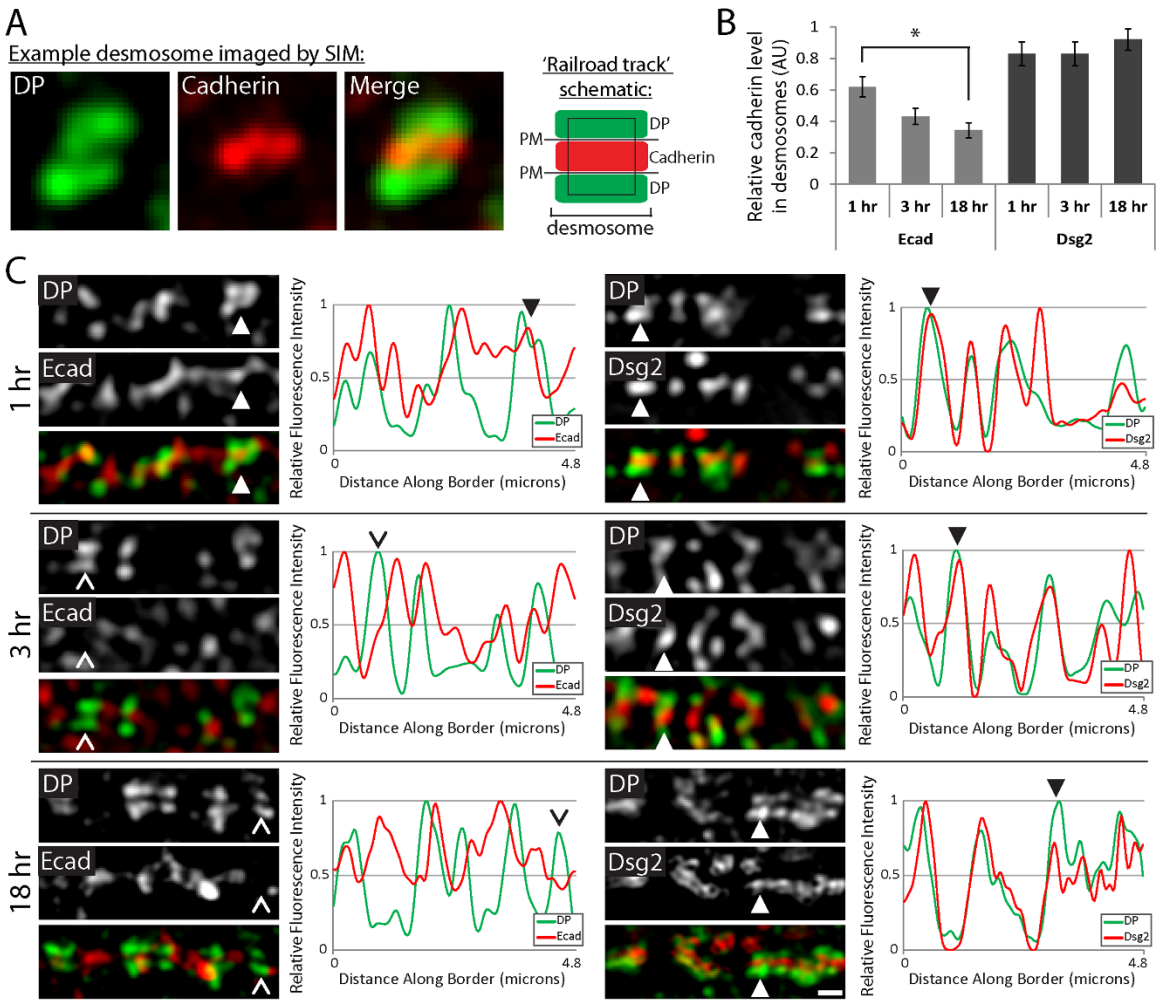

Figure 3.3: Ecad and Dsg2 are both localized in nascent desmosomes: (A) Analysis of cadherin localization within desmosomes. Structured illumination microscopy (SIM) is able to resolve the distance from plaque to plaque when desmosomes are stained with a C-terminal DP antibody and an N-terminal cadherin antibody, as shown in the example SIM image (Figure 3A). Desmosomes were defined by regions of parallel DP staining, or 'railroad tracks'. DP (green) and cadherin (either Ecad or Dsg2, red) fluorescence intensity were measured within the desmosome region of interest (black rectangle). (B) Quantification of cadherin (Ecad or Dsg2) levels relative to DP in desmosomes at different time points after initiation of desmosome assembly with high Ca^{2+} culture conditions. AU, arbitrary units. Means ± SE, n = 25 desmosomes, * $p < 0.05$. (C) Representative images and corresponding line scans of cell border regions of human keratinocytes cultured in high Ca^{2+} media for 1, 3 or 18 hrs. Images are oriented with cell borders horizontal. Scale bar, 0.5 µm. Solid arrowheads highlight desmosomes with cadherin staining while open arrowheads highlight desmosomes lacking cadherin staining.

3.3.4 Leu 175 mediates Ecad and Dsg2 interactions

Next, we proceeded to use single molecule AFM measurements to determine the precise molecular interactions that mediate Ecad/Dsg2 binding. Ecad can interact laterally to form *cis* dimers on the same cell surface [29] while Ecad molecules from opposing cells interact in a *trans* strand-swap dimer conformation [30-32] and a *trans* X-dimer conformation [33,34]. We therefore used mutants that specifically abolish either Ecad *trans* or *cis* interactions and tested their binding to Dsg2. Structural studies show that *trans* strand-swap dimer formation can be eliminated by mutating a conserved Trp2 (W2) to Ala (W2A) [34]. Similarly, mutating a conserved Lys14 to Glu (K14E) eliminates a key salt-bridge in the X-dimer interface and abolishes X-dimer formation [34]. We therefore tested the binding between the Ecad W2A-K14E

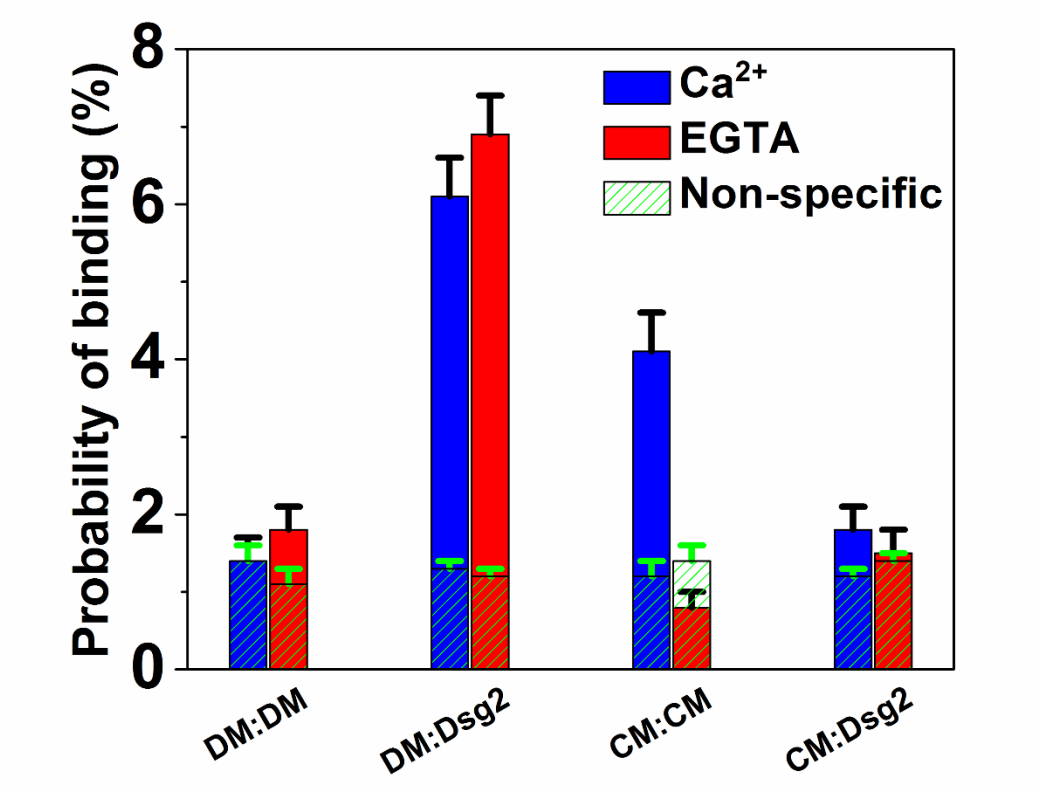

Figure 3.4: Ecad interacts with Dsg2 via Leu 175: Homophilic binding probability of Ecad W2A-K14E double mutant (DM); heterophilic binding probability of DM and Dsg2; homophilic binding probability of Ecad L175D *cis* dimer mutant (CM); and the

heterophilic binding probability of CM and Dsg2 was measured in Ca^{2+} (blue) and in EGTA (red). Nonspecific binding probabilities determined from the average of measured binding probabilities between a cadherin functionalized AFM tip and a bare surface and between a bare AFM tip and surface functionalized with biotinylated cadherins are shown in shaded green. DM/DM data was from a total of 1898 (Ca^{2+}) and 2122 (EGTA) measurements; DM/Dsg2 data was from a total of 2150 (Ca^{2+}) and 2009 (EGTA) measurements; CM/CM data was from a total of 1970 (Ca^{2+}) and 1906 (EGTA) measurements; CM/Dsg2 data was from a total of 2027 (Ca^{2+}) and 2122 (EGTA) measurements. Error bars are s.e. calculated using bootstrap with replacement**.**

double mutant (DM) and Dsg2. In agreement with previous results [19,34], we confirmed that the DM cannot interact homophilically; binding interaction between opposing DMs (1.4 ± 0.3% in Ca^{2+} and 1.8 ± 0.3% in EGTA) were comparable to nonspecific binding in Ca^{2+} (1.4 ± 0.1 %) and in EGTA (1.1 ± 0.1%) (Figure 3.4). However, when we measured the interactions between the DM on AFM tip and Dsg2 on CS, our data showed that the DM interacts with Dsg2 in a Ca^{2+}-independent heterophilic fashion; while the DM/Dsg2 binding probability in Ca^{2+} and in EGTA was 6.1 ± 0.5% and 6.9 ± 0.5% respectively, the non-specific interaction in Ca^{2+} and EGTA was 1.3 ± 0.1% and 1.2 ± 0.1% respectively (Figure 3.4). This demonstrates that the Ecad/Dsg2 binding interface is different from the previously established interface for Ecad *trans* dimerization.

Next, we tested whether Ecad interacts with Dsg2 via its *cis* dimer interface. Since previous studies had shown that mutating a conserved Leu 175 to Asp (L175D) eliminates Ecad *cis* dimerization [29], we measured the interaction of this Ecad *cis* mutant (CM) and Dsg2. First, we confirmed that CM was functional by measuring its *trans* binding probability. As shown previously [29], our data confirmed that the CM forms Ca^{2+}-dependent *trans* dimers; the binding probabilities in Ca^{2+} and in EGTA were 4.1 ± 0.5% and 0.8 ± 0.2% respectively (corresponding nonspecific binding probabilities in Ca^{2+} and in EGTA were 1.2 ± 0.2% and 1.4 ± 0.2% respectively) (Figure 3.4). However, the interaction of CM (on CS) and Dsg2 (on AFM tip) was comparable to the measured nonspecific binding; we measured binding

probabilities of 1.8 ± 0.3% in Ca^{2+} and 1.5 ± 0.3% in EGTA which were similar to measured nonspecific binding levels of 1.2 ± 0.1% in Ca^{2+} and 1.4 ± 0.1% in EGTA (Figure 3.4). Previous simulations [35,36] and single molecule FRET experiment [21] have shown that *cis* homo-dimerization of Ecad requires prior *trans* dimer formation. Thus, the failure to form CM/Dsg2 interactions is not due to the abrogation of Ecad *cis* dimers. Taken together, these experiments show that Ecad/Dsg2 dimerization is mediated by L175, which also mediates *cis* homo-dimerization in Ecad.

3.3.5 Ecad L175 is essential for efficient intercellular Dsg2 recruitment and desmosome assembly

To test whether the Ecad L175D mutation can impede recruitment of Dsg2 in keratinocytes, we expressed either full-length Ecad WT or mutants in E^{KO}/P^{KD} keratinocytes and analyzed Dsg2 recruitment to sites of intercellular contacts. We have previously shown that the E^{KO}/P^{KD} keratinocytes are unable to assemble adherens junction (AJs) and desmosomes due to the loss of all classical cadherins [14]. As we wanted to assess the ability of Ecad mutants to recruit desmosomal proteins early during junction formation, we performed confocal microscopy on keratinocytes immunostained for Ecad, Dsg2 and DP, at three time points following the Ca^{2+} switch (3 hr, 6 hr and 18 hr, Methods). In agreement with previous results [37], our data showed that 3 hr after the Ca^{2+} switch, 93% of WT-Ecad was enriched in zipper-like early AJs at sites of intercellular contacts. In contrast only 48% of L175D-Ecad transfected keratinocytes formed AJ zippers, likely due to impaired Ecad *cis*-dimer formation (Figure 3.5 A, B) [29]. At these early time points following the Ca^{2+} switch, 66% of the WT Ecad zipper contacts were positive for Dsg2. The junctional localization of Ecad and Dsg2 increased

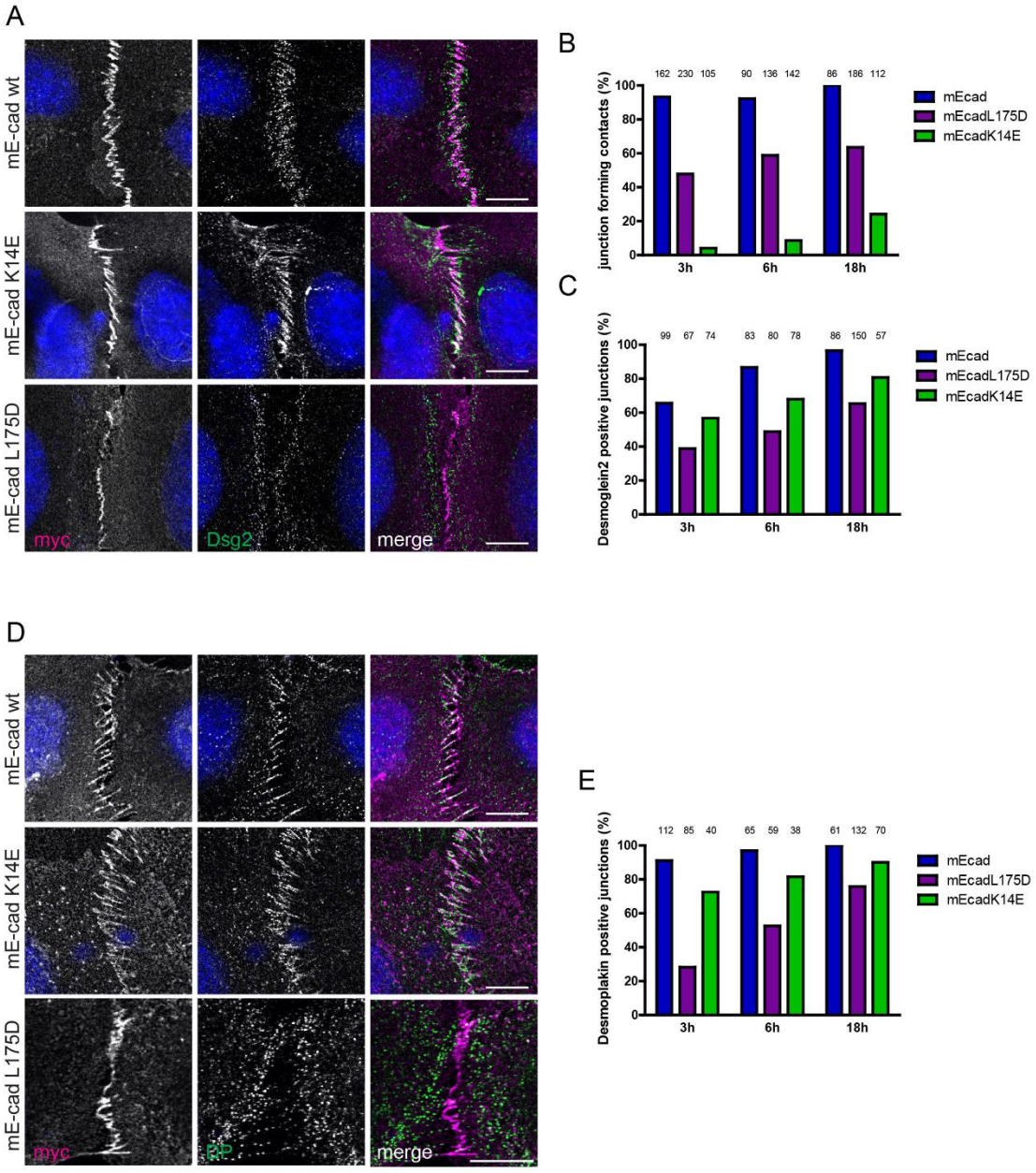

Figure 3.5: Ecad L175 promotes desmosome assembly in cells. (A) Immunofluorescence analysis for transfected WT or mutant Ecad (myc) and Dsg2, 6 hr after allowing de novo junction formation in Ecad^{KO}/Pcad^{KD} keratinocytes. Note decreased localization of Dsg2 and intercellular contacts formed by L175D-Ecad. (B) Quantification of adherens junction (AJ) formation at intercellular contacts, judged by zipper-like enrichment of Ecad constructs. (C) Quantification of Dsg2 co-enrichment at AJ formed by WT or mutant Ecad. (D) Immunofluorescence analysis for transfected WT or mutant Ecad (myc) and desmoplakin (DP), 6 hr after allowing de novo junction formation in Ecad^{KO}/Pcad^{KD} keratinocytes. Note

decreased localization of DP and intercellular contacts formed by L175D-Ecad. (E) Quantification of DP co-enrichment at AJ formed by WT or mutant Ecad. Numbers of quantified junctions (interface of two contacting, transfected cells) are shown above each bar. Scale bar: 10μm.

to 97%, 18 hr after allowing cells to engage in Ca^{2+}-dependent intercellular adhesion (Figure 3.5 A, C). In contrast, only 39% of L175-induced zipper contacts showed Dsg2 recruitment 3 hr after switching to high Ca^{2+} (Figure 3.5 A, C), which increased to 65% at 18 hr, confirming that a direct interaction between Ecad and Dsg2 is required for efficient recruitment of Dsg2 to early intercellular contacts.

To confirm that the observed effect of the L175D mutation was not due to hindered AJ formation, we transfected the E^{KO}/P^{KD} keratinocytes with the full-length Ecad-K14E mutant that abolishes X-dimer formation and traps Ecad in a strand-swap dimer conformation [19,34]. Our data showed that only 4% of the transfected, contacting cells formed zippers at early (3 hr) time-points after switching to high Ca^{2+} with only 24% of the transfected contacting cells showing zippers at late (18 hr) time points (Figure 3.5 A, B, figure supplement 1), confirming that K14 is essential for effective AJ formation [38], and thus intercellular contact establishment. However, the few K14E AJs that were formed, recruited Dsg2 more efficiently than L175D (Figure 3.5 A, C, figure supplement 1). This result confirmed that delayed recruitment of Dsg2 to inter-cellular contacts was not the result of the inability of the Ecad L175D to efficiently form AJs but rather due to absence of direct interaction between Ecad and Dsg2. That there was no co-localization of DP and Ecad in the absence of zippers (Figure 3.5 supplement 1) suggests that Ecad *trans* interactions precede Ecad/Dsg2 interactions. This conclusion is further strengthened by our finding that no DP recruitment was observed upon abolishing Ecad *trans* adhesion, and thus zippers, by transfecting the full-length Ecad-DM (W2A-K14E double mutant, Figure 3.5 supplement 1) in E^{KO}/P^{KD} keratinocytes.

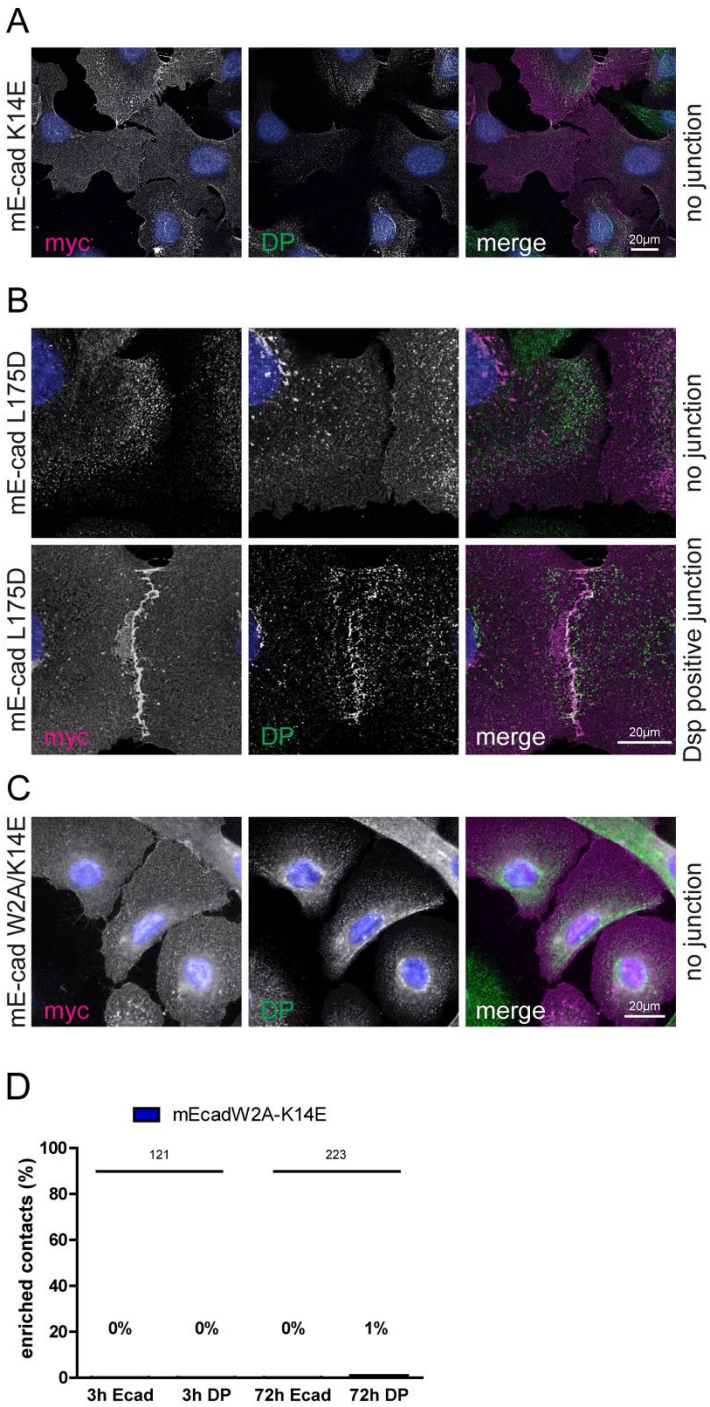

Figure 3.5 supplement 1: Impaired junction formation in Ecad-K14E, Ecad-L175D, and Ecad-W2A/K14E (DM) mutants. Immunofluorescence analysis for transfected Ecad-K14E, Ecad-L175D, Ecad-DM, and desmoplakin (DP), 6 hr after de novo junction formation in $Ecad^{KO}/Pcad^{KD}$ keratinocytes. (A) Example for Ecad-K14E transfected contacting cells that

do not form strand-swap dimer mediated AJ zippers. (B) Upper panel: example for Ecad-L175D transfected contacting cells that do not form AJ zippers. Lower panel: example for Ecad L175D mediated AJ zippers that were counted as DP positive. (C) Example for Ecad-DM transfected contacting cells that do not form AJ zippers. (D) Quantification of AJ formation and DP recruitment at intercellular contacts of DM transfected cells. Numbers of quantified junctions (interface of two contacting, transfected cells) are shown above each bar.

Finally, to examine whether L175D only interferes with Dsg2 recruitment or more generally delays desmosome assembly, we also examined the ability of L175D-Ecad to hinder DP recruitment. Our data showed that in E^{KO}/P^{KD} keratinocytes transfected with WT-Ecad, DP was enriched in 91% of intercellular contacts after 3 hr in high Ca^{2+} and in 100% of contacts after 18 hr (Figure 3.5 D, E). In contrast, after 3 hr, only 28% of L175D-Ecad mutant established intercellular contacts were positive for DP, which was increased to 72% after 18 hr, suggesting a compensatory mechanism at later stages. Importantly, after 3 hr, 73% of K14E-Ecad mutant contacts were DP positive, despite widespread defects in AJ formation (Figure 3.5 B, D, E). Taken together these results confirm that amino acid L175 in Ecad mediates Dsg2 interactions and facilitates early desmosome complex formation in cells.

3.4 Discussion

Here, we used an approach that integrates *in vitro* single molecule and cellular structure-function experiments to identify two critical events that initiate and promote efficient desmosome assembly: *(i)* stable *trans*-homodimerization of Ecad, and *(ii)* the direct heterophilic binding of Ecad and Dsg2 ectodomains. Our data demonstrates that desmosome assembly is initiated at sites of Ecad *trans* homodimerization. Subsequently, Ecad and Dsg2 bind via a conserved Leu 175 on the Ecad *cis* binding interface and form short-lived heterophilic complexes that localize to early desmosomes and efficiently recruit desmosomal proteins to sites of intercellular contact formation. As desmosomes mature, Dsg2 dissociates from Ecad and forms stable bonds with Dsc2 to mediate robust adhesion.

Previously, biochemical analysis identified Ecad/Dsg and Dsc/Dsg complexes upon removing Ca^{2+} from the cell culture [39]. Our data builds upon these previous findings by showing a direct interaction between Ecad and Dsg that also occurs under conditions that promote intercellular adhesions and by identifying the Ecad interface responsible for the interaction. We also demostrate that in a physiological setting, L175 on Ecad is important for recruitment of Dsg2 and DP and for efficient desmosome formation. It has also been suggested that cross-talk between classical and desmosomal cadherins is mediated by plakoglobin, a cytoplasmic signaling protein found in both AJs and desmosomes [40]. While we did not test the role of plakoglobin in desmosome formation, our data indicates that a direct physical interaction between Ecad and Dsg2 is critical for timely desmosome assembly. It is important to point out that Ecad/Dsg interactions reported here may not be unique to Dsg2 but may occur with other Dsg isoforms as well. In keratinocytes, Dsg3 is essential for desmosome assembly [41,42] and a previous fluorescence co-localization and co-immunoprecipitation study reported interactions between Ecad and Dsg3 [43]. Since the E^{KO}/P^{KD} keratinocytes transfected with Ecad L175D also express Dsg3, it is possible that poor junctional DP enrichment seen at early time-points, which was more impaired than Dsg2 recruitment, may result from the inability of EcadL175 to bind Dsg3.

Desmosome assembly is Ca^{2+} dependent and previous models using Dsc2 and Dsg2 propose that desmosomal cadherins assemble in two phases [17,44]. The first phase of assembly is believed to involve the clustering of Dsc into nucleation sites. Since Dsc2 homo-dimerization is Ca^{2+} dependent (Figure 3.1E), it follows that desmosome assembly requires Ca^{2+}, even though Dsc2/Dsg2 heterodimers are Ca^{2+} independent. In the second phase of desmosome formation, Dsg2 is recruited to the clustered Dsc2 nucleation sites through an unknown mechanism that is Ca^{2+} and W2 independent and that relies on heterophilic interactions with other proteins [17]. Our data suggests that Ecad mediates Ca^{2+} independent recruitment of

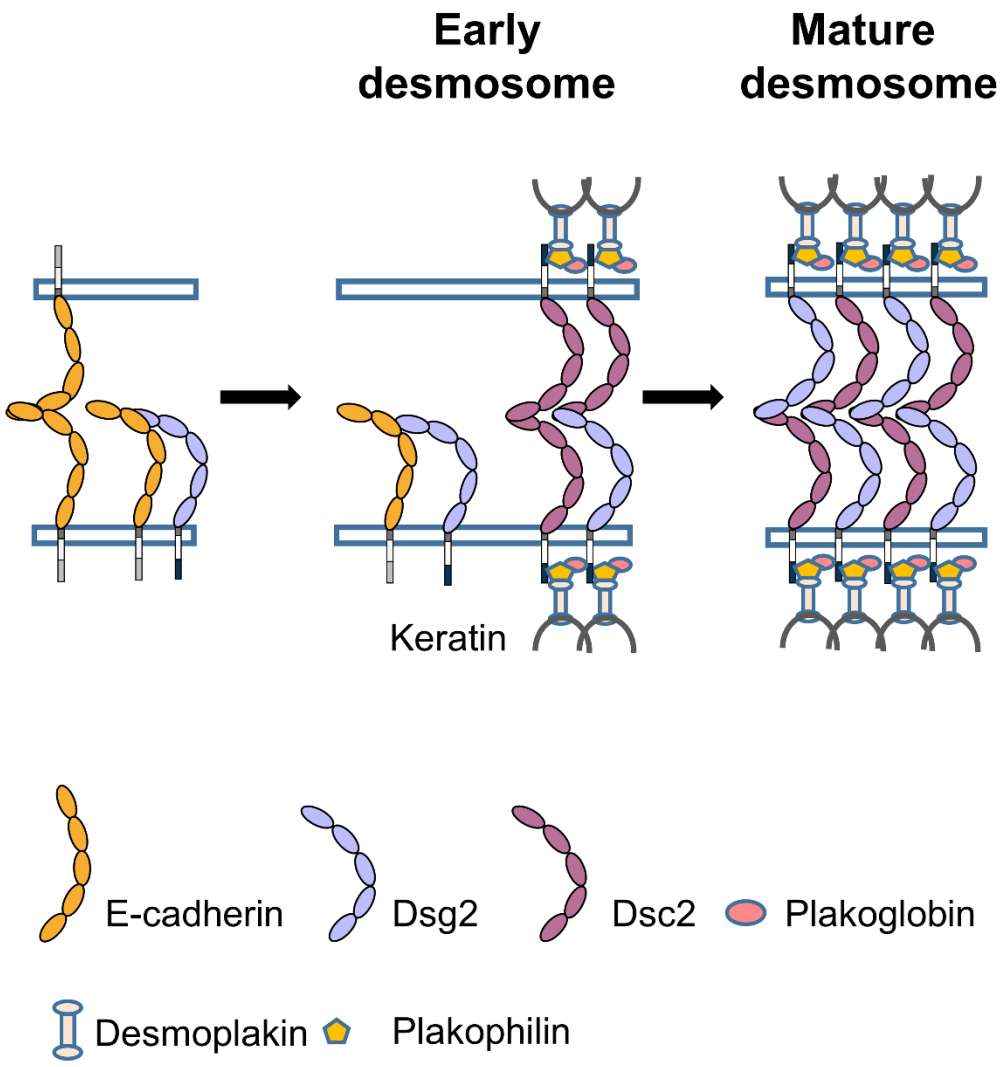

Figure 3.6: Proposed model for the role of Ecad in desmosome assembly: Ecad (orange) interacts with Dsg2 (light blue) to form a low-lifetime *cis* heterodimer. Formation of Ecad/Dsg2 complex requires prior Ecad *trans* homodimerization. The Ecad/Dsg2 complex is incorporated in the nascent desmosome which also contains low-lifetime Dsc2/Dsc2 dimers (purple). As the desmosome matures, the Ecad/Dsg2 heterodimers and Dsc2/Dsc2 homodimers dissociate. The Dsg2 and Dsc2 interact to form a robust, high-lifetime, *trans* adhesive complex

Dsg2, and perhaps other Dsgs, to nascent Dsc clusters. Previous studies have also shown that initial cell-cell contacts subsequently trigger multiple phases of DP recruitment to finally assemble desmosomes [45].

Although our biophysical experiments demonstrate that Ecad-DM directly interact with Dsg2, imaging of keratinocytes transfected with Ecad-K14E and Ecad-DM show that stable *trans*-Ecad homodimerization is required for DP and Dsg2 recruitment (Figure 3.5 supplement 1). While the K14E mutants are strongly impaired in AJ zipper formation, they only localize with Dsg2 or DP when AJ zippers are present. Similarly, cells expressing Ecad-DM which do not form AJs, also do not recruit DP or Dsg2. These results indicate that Ecad *trans* binding serves as the initial spatial cue for the subsequent recruitment of Dsg2 and consequently for desmosome assembly. These results are thus in line with the observation that combined loss of both E-, and P-cadherin, the two main cadherins expressed in keratinocytes, prevents desmosome assembly [14]. Mechanistically, the cross talk between Ecad *trans* dimerization and Ecad/Dsg2 binding may be analogous to Ecad *cis* homodimerization via L175, which occurs only when conformational entropy is reduced by prior Ecad *trans* binding [35,36]. Alternatively, Ecad *trans* dimers may be needed to bring opposing cells closer together to initiate desmosome formation. In support of this possibility, a previous study has suggested that when opposing HeLa cell membranes are brought into close proximity, by the interaction of protein zero neuronal adhesion molecules, desmosomes are formed [46].

Based on these previous studies and our new data, we propose a model (Figure 3.6) whereby desmosome assembly is facilitated both by the direct *cis* interactions of classical cadherins and Dsg and the *trans* binding of opposing classical cadherins. In our model, the *trans* homodimerization of Ecad from opposing cells serves as a spatial cue to coordinate desmosome assembly. Ecad subsequently forms *cis* dimer complexes with Dsg though the results presented here do not rule out Ecad/Dsg binding in a *trans* conformation. Importantly,

the data suggest that once localized within the native desmosome, Dsg dissociates from Ecad and binds to Dsc to form mature desmosomes. Since the Dsc2/Dsg2 complex has a longer lifetime than both the Ecad/Dsg2 complex and Dsc2/Dsc2 complex, the Dsg/Dsc interactions likely promotes robust cell-cell adhesion and permits the mature desmosome to withstand mechanical force.

3.5 Materials and Methods

3.5.1 Purification of cadherin ectodomains

The generation of HEK293T cells stably expressing WT-Ecad and Ecad W2A-K14E fused to a C-terminal Avi-tag and His-tag have been described previously [19,21]. Plasmids for full length Dsc2 and Dsg2 ectodomains fused to a C-terminal Avi-tag and His-tag were a kind gift from Prof. W. James Nelson (Stanford University) while HEK293T cells stably expressing full-length Ecad mutant L175D fused to a C-terminal Avi-tag and His-tag were a kind gift from Dr. Yunxiang Zhang (Stanford University). As described previously [17], the Dsc2 and Dsg2 plasmids were transiently transfected into HEK 293T cells using lipofactamine 2000 (Life Technologies) following the manufacturer's protocol. Two days post transfection, the conditioned media was collected for protein purification. The transfected cells expressing WT/mutant Ecads were grown to confluence in DMEM containing 10% FBS and 200 µg/ml of Genecitin (G418; Invitrogen) and exchanged into serum free DMEM with 400 µg/ml of Genecitin. Conditioned media was collected 4 days after media exchange.

Purification and biotinylation of His-tagged Dsc2, Dsg2, WT-Ecad, W2A-K14E, and L175D followed a protocol that has been described previously [17,19,21]. Media containing cadherin was incubated overnight, at 4 ºC, with Ni NTA agarose beads (Qiagen). The beads were loaded onto a glass chromatography column (BioRad) and washed with buffer at pH 7.5 (20 mM NaH_2PO_4, 500 mM NaCl and 1 mM $CaCl_2$) containing 50 mM imidazole. The bound

protein was eluted with the same buffer containing 250 mM imidazole. Following purification, the protein was exchanged into a pH 7.5 buffer containing 25 mM Hepes, 5 mM NaCl, and 1 mM $CaCl_2$ and biotinylated with BirA enzyme (BirA500 kit; Avidity). After biotinylation for 1 hr at 30 °C, free biotins were removed using either a spin column (Millipore) or superdex 200 10/300 GL column.

3.5.2 Single molecule AFM force measurements

Purified cadherins were immobilized on coverslips (CS) and AFM cantilevers (Olympus, model TR400PSA) using a previously described method [47]. Briefly, the CS and cantilevers were cleaned with 25% H_2O_2:75% H_2SO_4 and washed with DI water. The CS was then cleaned with 1 M KOH and washed with DI water. Both the CS and cantilevers were washed with acetone and functionalized using 2% (v/v) 3-aminopropyltriethoxysilane (Sigma) dissolved in acetone. Next, N-hydroxysuccinimide ester functionalized PEG spacers (MW 5000, Lysan Bio) were covalently attached to the silanized AFM tip and coverslip; 7% of the PEG spacers were decorated with biotin groups. Prior to a measurement, the functionalized AFM cantilever and coverslip were incubated overnight with BSA (1 mg/ml) to further reduce non-specific binding. The tip and surface were then incubated with 0.1 mg/ml streptavidin for 30 minutes and biotinylated cadherins were attached to the streptavidin. Finally, the surfaces were incubated with 0.02 mg/ml biotin for 10 minutes to block the free biotin binding sites on streptavidin.

Force measurements were performed using an Agilent 5500 AFM with a closed loop scanner. The spring constants of the cantilevers were measured using the thermal fluctuation method [48]. All the experiments were performed in a pH 7.5 buffer containing 10 mM Tris-HCl, 100 mM NaCl and 10 mM KCl with either 2.5 mM Ca^{2+} or 2 mM EGTA. The region of PEG stretching in each unbinding force curve was fit to an extended freely jointed chain model

using a total least squares fitting protocol. The contour length L_c of the PEG tethers was determined from the fits. The histogram of L_c for each experiment was fit to a Gaussian distribution and only force curves that had an L_c within one standard deviation from the center were accepted for further analysis. Loading rates were calculated as described elsewhere [49]. K-means clustering method was used to group loading rates [25]. Mean force F^* and mean loading rate r_f were calculated for each group and plots of F^* vs. r_f were fit using nonlinear least-squares fitting with bisquare weights to the Bell-Evans model [23,24]. Confidence intervals (CIs) for k_{off}^0 and x_β were determined using bootstrap-with-replacement, as described previously [50].

3.5.3 SIM imaging and analysis of cadherin localization within desmosomes

Primary human keratinocytes (HKs, passage 2) were isolated from neonatal foreskin as previously described [51] and cultured in KBM-Gold basal medium (100 µM calcium) supplemented with KGM-Gold Single-Quot Kit (Lonza, Walkersville, MD). HKs were cultured to 70% confluence on glass coverslips, switched to 550 µM calcium to induce junction assembly for the various time points indicated and then processed for structured illumination microscopy (SIM) as described below.

HKs were fixed in methanol and immunostained with primary antibodies for 1 h and secondary antibodies for 30 min, both at 37 °C. The following primary antibodies were used in the SIM experiments: mouse anti-Ecad antibody (HECD-1, Abcam); rat anti-uvomorulin (DECMA-1, Sigma); mouse anti-Dsg2 antibody (AH12.2, a kind gift from Dr. Asma Nusrat, Emory University); desmoplakin antibody (NW6, a kind gift from Dr. Kathleen Green, Northwestern University). Secondary antibodies conjugated to Alexa Fluorophore were purchased from Invitrogen. SIM was performed using the Nikon N-SIM system on an Eclipse Ti-E microscopy system equipped with a 100x/1.49 NA oil immersion objective and 488 and

561 nm solid-state lasers. 3D SIM images were captured with an EM charge-coupled device camera (DU-897, Andor Technology) and reconstructed using NIS-Elements software with the N-SIM module (version 3.22, Nikon).

SIM is able to resolve the distance from plaque to plaque when desmosomes are stained with a C-terminal DP antibody and an N-terminal cadherin antibody, as shown in the example SIM image (Figure 3A). For analysis of cadherin localization within desmosomes, desmosomes were first defined by regions of parallel DP staining, or 'railroad tracks'. Using ImageJ, a desmosome region of interest (black rectangle) was identified via DP staining (Figure 3A). Once a DP and 'railroad track'-positive region of interest was identified, cadherin (red) fluorescence intensity levels were then independently measured along with DP (green) levels. Pairwise multiple comparisons were performed via a Tukey test with a significance level of $\alpha = 0.05$.

3.5.4 Isolation, culture, transfection and confocal imaging of primary keratinocytes

Spontaneously immortalized primary keratinocytes, isolated from newborn mice, were cultured in DMEM/HAM's F12 (FAD) medium with low Ca^{2+} (50 µM) (Biochrom) supplemented with 10 % FCS (chelated), penicillin (100 U ml^{-1}), streptomycin (100 µg ml^{-1}, Biochrom A2212), adenine (1.8×10^{-4} M, SIGMA A3159), L-glutamine (2mM, Biochrom K0282), hydrocortisone (0.5 µg ml^{-1}, Sigma H4001), EGF (10 ng ml^{-1}, Sigma E9644), cholera enterotoxin (10^{-10} M, Sigma C-8052), insulin (5 µg ml^{-1}, Sigma I1882), and ascorbic acid (0.05 mg ml^{-1}, Sigma A4034). Keratinocytes were kept at 32°C and 5% CO_2. $Ecad^{KO}$/$Pcad^{KD}$ cells were generated by lentiviral transduction of Ecad-deficient keratinocytes using C14 shRNA directed against Pcad [14]. Cultured cells were regularly monitored for mycoplasma contamination and discarded in case of positive results.

Ecad-K14E and Ecad-L175D mutants were generated using WT mouse Ecad cDNA in a pcDNA3 backbone including a c-terminal 6myc-tag. Mutations were carried out using “QuikChange Lightning Site-Directed Mutagenesis Kit” (Agilent). Keratinocytes were transfected at 80-100% confluency with Viromer®Red (lipocalyx) according to the manufacturer’s protocol. In brief 1.5µg DNA were diluted in 100µl Buffer, added to 1.25µl Viromer®RED and incubated for 15min at room temperature. Approximately 33µl transfection mix were used per well (24 well plate).

Confocal images were obtained with a Leica TCS SP8, equipped with a white light laser and gateable hybrid detectors (HyDs) and a PlanApo 63x, 1.4 NA objective. Epifluorescence images were obtained with a Leica DMI6000 with a PlanApo 63x, 1.4 NA objective. The following primary antibodies were used in this study: rabbit monoclonal against Dsg2 (1:500, Abcam #ab150372); mouse monoclonal against DP1/2 (1:200, Progen #61003); mouse monoclonal against c-myc (IF 1:2000, Cell Signaling #2276); Secondary antibodies were species-specific antibodies conjugated with either AlexaFluor 488, 594 or 647, used at a dilution of 1:500 for immunofluorescence (Molecular Probes, Life Technologies)

3.6 Acknowledgements

This research was supported in part by the American Heart Association (12SDG9320022), National Institute of General Medical Sciences of the National Institutes of Health (R01GM121885) and National Science Foundation (PHY-1607550) to SS; by the Deutsche Forschungsgemeinschaft (DFG SFB 829 A1, DFG SFB 829 Z2, DFG NI 1234/6-1) to CMN; and by the National Institute of Arthritis and Musculoskeletal and Skin Diseases of the National Institutes of Health (R01AR048266) to APK.

3.7 References

1 Brasch, J., Harrison, O. J., Honig, B. & Shapiro, L. Thinking outside the cell: how cadherins drive adhesion. *Trends in Cell Biology* **22**, 299-310, doi:10.1016/j.tcb.2012.03.004 (2012).

2 Rübsam, M. *et al.* Adherens junctions and desmosomes coordinate mechanics and signaling to orchestrate tissue morphogenesis and function: an evolutionary perspective. *Cold Spring Harbor Perspectives in Biology*, doi:10.1101/cshperspect.a029207 (2017).

3 Dusek, R. L., Godsel, L. M. & Green, K. J. Discriminating roles of desmosomal cadherins: Beyond desmosomal adhesion. *Journal of Dermatological Science* **45**, 7-21, doi:10.1016/j.jdermsci.2006.10.006 (2007).

4 Getsios, S., Huen, A. C. & Green, K. J. Working out the strength and flexibility of desmosomes. *Nat. Rev. Mol. Cell Biol.* **5**, 271-281, doi:10.1038/nrm1356 (2004).

5 Eshkind, L. *et al.* Loss of desmoglein 2 suggests essential functions for early embryonic development and proliferation of embryonal stem cells. *Eur. J. Cell Biol.* **81**, 592-598, doi:10.1078/0171-9335-00278 (2002).

6 Awad, M. M. *et al.* DSG2 Mutations Contribute to Arrhythmogenic Right Ventricular Dysplasia/Cardiomyopathy. *American Journal of Human Genetics* **79**, 136-142 (2006).

7 Syrris, P. *et al.* Arrhythmogenic Right Ventricular Dysplasia/Cardiomyopathy Associated with Mutations in the Desmosomal Gene Desmocollin-2. *American Journal of Human Genetics* **79**, 978-984 (2006).

8 Green, K. J. & Simpson, C. L. Desmosomes: New Perspectives on a Classic. *Journal of Investigative Dermatology* **127**, 2499-2515, doi:10.1038/sj.jid.5701015 (2007).

9 Amagai, M. & Stanley, J. R. Desmoglein as a Target in Skin Disease and Beyond. *J. Invest. Dermatol.* **132**, 776-784, doi:10.1038/jid.2011.390 (2012).

10 Jones, J. C. Characterization of a 125K glycoprotein associated with bovine epithelial desmosomes. *J. Cell Sci.* **89**, 207-216 (1988).

11 Gumbiner, B., Stevenson, B. & Grimaldi, A. The role of the cell adhesion molecule uvomorulin in the formation and maintenance of the epithelial junctional complex. *The Journal of Cell Biology* **107**, 1575-1587 (1988).

12 Lewis, J. E., Jensen, P. J. & Wheelock, M. J. Cadherin function is required for human keratinocytes to assemble desmosomes and stratify in response to calcium. *The Journal of Investigative Dermatology* **102**, 870-877, doi:10.1111/1523-1747.ep12382690 (1994).

13 Wheelock, M. J. & Jensen, P. J. Regulation of keratinocyte intercellular junction organization and epidermal morphogenesis by E-cadherin. *The Journal of Cell Biology* **117**, 415-425, doi:10.1083/jcb.117.2.415 (1992).

14 Michels, C., Buchta, T., Bloch, W., Krieg, T. & Niessen, C. M. Classical Cadherins Regulate Desmosome Formation. *J. Invest. Dermatol.* **129**, 2072-2075, doi:10.1038/jid.2009.17 (2009).

15 Amagai, M. *et al.* Delayed Assembly of Desmosomes in Keratinocytes with Disrupted Classic-Cadherin-Mediated Cell Adhesion by a Dominant Negative Mutant. *Journal of Investigative Dermatology* **104**, 27-32, doi:10.1111/1523-1747.ep12613462 (1995).

16 Tinkle, C. L., Pasolli, H. A., Stokes, N. & Fuchs, E. New insights into cadherin function in epidermal sheet formation and maintenance of tissue integrity. *Proceedings of the National Academy of Sciences* **105**, 15405-15410, doi:10.1073/pnas.0807374105 (2008).

17 Lowndes, M. *et al.* Different roles of cadherins in the assembly and structural integrity of the desmosome complex. *Journal of Cell Science* **127**, 2339-2350, doi:10.1242/jcs.146316 (2014).

18 Manibog, K., Li, H., Rakshit, S. & Sivasankar, S. Resolving the molecular mechanism of cadherin catch bond formation. *Nature Communications* **5**, doi:10.1038/ncomms4941 (2014).

19 Rakshit, S., Zhang, Y., Manibog, K., Shafraz, O. & Sivasankar, S. Ideal, catch, and slip bonds in cadherin adhesion. *Proceedings of the National Academy of Sciences* **109**, 18815-18820, doi:10.1073/pnas.1208349109 (2012).

20 Sivasankar, S., Zhang, Y., Nelson, W. J. & Chu, S. Characterizing the Initial Encounter Complex in Cadherin Adhesion. *Structure* **17**, 1075-1081, doi:10.1016/j.str.2009.06.012 (2009).

21 Zhang, Y., Sivasankar, S., Nelson, W. J. & Chu, S. Resolving cadherin interactions and binding cooperativity at the single-molecule level. *Proceedings of the National Academy of Sciences of the United States of America* **106**, 109-114, doi:10.1073/pnas.0811350106 (2009).

22 Oesterhelt, F., Rief, M. & Gaub, H. E. Single molecule force spectroscopy by AFM indicates helical structure of poly(ethylene-glycol) in water. *New Journal of Physics* **1**, 6, doi:10.1088/1367-2630/1/1/006 (1999).

23 Bell, G. I. Models for the specific adhesion of cells to cells. *Science* **200**, 618-627, doi:10.1126/science.347575 (1978).

24 Evans, E. & Ritchie, K. Dynamic strength of molecular adhesion bonds. *Biophys. J.* **72**, 1541-1555 (1997).

25 Yen, C.-F. & Sivasankar, S. Improving estimation of kinetic parameters in dynamic force spectroscopy using cluster analysis. *The Journal of Chemical Physics* **148**, 123301, doi:10.1063/1.5001325 (2018).

26 Harrison, O. J. *et al.* Structural basis of adhesive binding by desmocollins and desmogleins. *Proceedings of the National Academy of Sciences* **113**, 7160-7165, doi:10.1073/pnas.1606272113 (2016).

27 Stahley, S. N., Bartle, E. I., Atkinson, C. E., Kowalczyk, A. P. & Mattheyses, A. L. Molecular organization of the desmosome as revealed by direct stochastic optical reconstruction microscopy. *J Cell Sci*, doi:10.1242/jcs.185785 (2016).

28 Stahley, S. N. *et al.* Super-Resolution Microscopy Reveals Altered Desmosomal Protein Organization in Tissue from Patients with Pemphigus Vulgaris. *Journal of Investigative Dermatology* **136**, 59-66, doi:10.1038/JID.2015.353 (2016).

29 Harrison, O. J. *et al.* The Extracellular Architecture of Adherens Junctions Revealed by Crystal Structures of Type I Cadherins. *Structure* **19**, 244-256, doi:10.1016/j.str.2010.11.016 (2011).

30 Boggon, T. J. *et al.* C-Cadherin Ectodomain Structure and Implications for Cell Adhesion Mechanisms. *Science* **296**, 1308-1313, doi:10.1126/science.1071559 (2002).

31 Parisini, E., Higgins, J. M. G., Liu, J.-h., Brenner, M. B. & Wang, J.-h. The Crystal Structure of Human E-cadherin Domains 1 and 2, and Comparison with other Cadherins in the Context of Adhesion Mechanism. *J. Mol. Biol.* **373**, 401-411, doi:10.1016/j.jmb.2007.08.011 (2007).

32 Vendome, J. *et al.* Molecular design principles underlying β-strand swapping in the adhesive dimerization of cadherins. *Nat. Struct. Mol. Biol.* **18**, 693-700, doi:10.1038/nsmb.2051 (2011).

33 Ciatto, C. *et al.* T-cadherin structures reveal a novel adhesive binding mechanism. *Nature Structural & Molecular Biology* **17**, 339-347, doi:10.1038/nsmb.1781 (2010).

34 Harrison, O. J. *et al.* Two-step adhesive binding by classical cadherins. *Nature Structural & Molecular Biology* **17**, 348-357, doi:10.1038/nsmb.1784 (2010).

35 Wu, Y. *et al.* Cooperativity between trans and cis interactions in cadherin-mediated junction formation. *Proceedings of the National Academy of Sciences of the United States of America* **107**, 17592-17597, doi:10.1073/pnas.1011247107 (2010).

36 Wu, Y., Vendome, J., Shapiro, L., Ben-Shaul, A. & Honig, B. Transforming binding affinities from three dimensions to two with application to cadherin clustering. *Nature* **475**, 510-513 (2011).

37 Vasioukhin, V., Bauer, C., Yin, M. & Fuchs, E. Directed actin polymerization is the driving force for epithelial cell-cell adhesion. *Cell* **100**, 209-219, doi:10.1016/S0092-8674(00)81559-7 (2000).

38 Hong, S., Troyanovsky, R. B. & Troyanovsky, S. M. Cadherin exits the junction by switching its adhesive bond. *The Journal of Cell Biology* **192**, 1073 (2011).

39 Troyanovsky, R. B., Klingelhofer, J. & Troyanovsky, S. Removal of calcium ions triggers a novel type of intercadherin interaction. *J. Cell Sci.* **112**, 4379-4387 (1999).

40 Lewis, J. E. *et al.* Cross-Talk between Adherens Junctions and Desmosomes Depends on Plakoglobin. *The Journal of Cell Biology* **136**, 919-934, doi:10.1083/jcb.136.4.919 (1997).

41 Hartlieb, E. *et al.* Desmoglein 2 Is Less Important than Desmoglein 3 for Keratinocyte Cohesion. *PLOS ONE* **8**, e53739, doi:10.1371/journal.pone.0053739 (2013).

42 Koch, P. J. *et al.* Targeted Disruption of the Pemphigus Vulgaris Antigen (Desmoglein 3) Gene in Mice Causes Loss of Keratinocyte Cell Adhesion with a Phenotype Similar to Pemphigus Vulgaris. *The Journal of Cell Biology* **137**, 1091 (1997).

43 Tsang, S. M. *et al.* Desmoglein 3, via an interaction with E-cadherin, is associated with activation of Src. *Plos One* **5**, e14211, doi:10.1371/journal.pone.0014211 (2010).

44 Burdett, I. D. J. & Sullivan, K. H. Desmosome Assembly in MDCK Cells: Transport of Precursors to the Cell Surface Occurs by Two Phases of Vesicular Traffic and Involves Major Changes in Centrosome and Golgi Location during a Ca2+ Shift. *Exp. Cell Res.* **276**, 296-309, doi:10.1006/excr.2002.5509 (2002).

45 Godsel, L. M. *et al.* Desmoplakin assembly dynamics in four dimensions: multiple phases differentially regulated by intermediate filaments and actin. *The Journal of Cell Biology* **171**, 1045-1059, doi:10.1083/jcb.200510038 (2005).

46 Doyle, J. P., Stempak, J. G., Cowin, P., Colman, D. R. & D'Urso, D. Protein zero, a nervous system adhesion molecule, triggers epithelial reversion in host carcinoma cells. *The Journal of Cell Biology* **131**, 465-482, doi:10.1083/jcb.131.2.465 (1995).

47 Manibog, K. *et al.* Molecular determinants of cadherin ideal bond formation: Conformation-dependent unbinding on a multidimensional landscape. *Proceedings of the National Academy of Sciences*, 201604012, doi:10.1073/pnas.1604012113 (2016).

48 Hutter, J. L. & Bechhoefer, J. Calibration of atomic-force microscope tips. *Rev. Sci. Instrum.* **64**, 1868-1873, doi:10.1063/1.1143970 (1993).

49 Ray, C., Brown, J. R. & Akhremitchev, B. B. Rupture Force Analysis and the Associated Systematic Errors in Force Spectroscopy by AFM. *Langmuir* **23**, 6076-6083, doi:10.1021/la070131e (2007).

50 Yen, C.-F., Harischandra, D. S., Kanthasamy, A. & Sivasankar, S. Copper-induced structural conversion templates prion protein oligomerization and neurotoxicity. *Sci. Adv.* **2**, e1600014, doi:10.1126/sciadv.1600014 (2016).

51 Calkins, C. C. *et al.* Desmoglein Endocytosis and Desmosome Disassembly Are Coordinated Responses to Pemphigus Autoantibodies. *J. Biol. Chem.* **281**, 7623-7634, doi:10.1074/jbc.M512447200 (2006).

CHAPTER 4. FAST FRAP TO STUDY ENDOCYTOSIS DRIVEN REMODELING OF ADHERENS JUNCTION

4.1 Introduction

The interplay between tissue mechanics and biochemical signaling orchestrate tissue morphogenesis and development [1]. Cadherin adherens junctions play a prominent role in this process by mediating a very dynamic assembly of intercellular connections [2]. One of the key mechanisms for modulating adhesion strength is the adjustment of the amount of cadherin present in the cellular junctions. This is achieved by endocytosis and degradation, which remove cadherin from the plasma membrane and synthesis and recycling, which increase the amount of cadherin available [3]. Dynamic aspects of cadherin based cell– cell adhesion are important during various morphogenetic events in development including epithelial mesenchymal conversions [4], gastrulation in a variety of organisms [5,6] and cell sorting [7]. Loss of adhesion in many types of cancer is often attributed to decreased E-cadherin expression due to genetic mutations [8] . There is evidence that downregulation and internalization of E-cadherin could significantly enhance the invasive ability of nasopharyngeal carcinoma [9]. Ultra-Violet radiation induced E-cadherin down regulation is shown in squamous cell cancers [10]. Src-dependent E-cadherin internalization with shear stress is believed to occur in metastatic oesophageal tumors [11]. Therefore, it is important to understand how amounts of E-cadherins in the intercellular junction are controlled. There are two views in the field: (i) cadherins are reorganized by reversible dissociation from a membrane cadherin cluster, followed by membrane diffusion, and new engagement into an adhesive cluster [12] and (ii) cadherins are trafficked by endocytosis and exocytosis dependent recycling [13].

The classical view is that Ecad exists as two pools: *trans* dimer Ecads bound to actin cytoskeleton via β-catenin, α-catenin and a monomer Ecad pool that are not bound to F-actin and exchanges with *trans* dimer pool [14]. Actin tethered proteins are confined by actin dynamics while the proteins that are not tethered to actin or monomers are free to undergo

brownian diffusion, but are corralled in the membrane because of the steric hindrance of the cytoplasmic domain of membrane proteins and the membrane [12,15,16]. Beads tagged with E/N-cadherins were shown transition from a freely diffusive stage to a cytoskeleton anchored state [16,17], also oligomerization of E-cad-GFP molecules on the free cell surface was found to dramatically decrease their brownian diffusion, strongly indicating a high degree of interaction with the membrane skeleton[15]. These results suggest diffusion is important for non-engaged cadherins while it is reduced when they are tethered to the cytoskeleton or when they are forming mature adherens junctions.

Cycles of endocytosis and recycling to the membrane have been also shown to play a major role in the local distribution of E-cadherin within mature adherens junctions [18]. It is well established that cadherins are internalized through endocytosis by several studies across various model organisms [19–22] which was initially reported for oxidative stress or extracellular calcium depletion in endothelial cells [23,24]. Cadherin endocytosis occurs through clathrin-mediated [25], caveolin mediated [26] or micropinocytosis [27,28] endocytosis pathways. In clathrin involved pathway, first the proteins are targeted for clathrin-mediated endocytosis by the binding of adaptor protein complexes; once bound, adaptor proteins recruit other components of the endocytic machinery and cluster into clathrin-coated pits [29]. Clathrin-coated pits containing proteins then undergo dynamin-mediated scission from the plasma membrane, budding off to form endocytic vesicles [30]. Studies have suggested that cadherin endocytosis may occur through caveolin-mediated pathway [26,31] where invagination of cholesterol-enriched microdomains within the plasma membrane that contain a coat protein known as caveolin, these structures are referred as lipid rafts or caveolae[32] ; and macropinocytosis pathway involves formation of large F-actin-coated vacuoles that serve to uptake either solid particles (phagosomes) or liquid (macropinosomes) from the extracellular space [33]. Though some of the specific details of the clathrin-independent pathways remain unclear, it appears that both clathrin-dependent and clathrin-independent endocytic pathways play a role in

cadherin turnover. It needs to be investigated whether different endocytosis pathways regulate tissue/cell specific internalization of cadherins or if they operate in the same cells but are activated by different signaling pathways.

While cadherins are internalized by endocytosis, they are introduced to the extracellular surface by exocytosis. Cadherins are synthesized and regulated at the endoplasmic reticulum (ER) [34,35], sorted at the trans-Golgi network (TGN)[36–38] and fused in to a recycling endosome [39]. Finally, cadherin carrying exocytosis vesicles are docked and fused with the plasma membrane [40]. Cadherin bearing vesicle fusion with the plasma membrane or exocytosis is a multistep process that is accomplished by the fusion of secretory vesicles with the plasma membrane catalyzed by the assembly of the SNARE complex and many other protein complexes [41–45].

While vesicle mediated endocytosis and exocytosis, carries cadherins in and out of the adherens junction, the biophysical details of this process are not well understood. For instance, the number of proteins each vesicle carries, its rate etc. are unknown. To understand the dynamics of this process, fluorescence recovery after photobleaching (FRAP) experiments have been widely used [46]. In a typical FRAP experiment, a small area on the sample with fluorescent molecules is photobleached by an intense, focused laser beam. The subsequent recovery of the fluorescence is monitored by the same, laser beam operating at a reduced intensity. Recovery occurs by replacement of the fluorophore in the bleached spot by transport from the surrounding regions. In a conventional set up, the recovery is determined by taking continues scanned images of an area that includes the photobleached region at a data acquisition rate of 1 frame/second.

This part of my thesis proposes a modified method to currently existing FRAP technique to extract dynamic details of the cellular junction using a custom built confocal

fluorescence set up operating with significantly higher data acquisition rates than used in regular FRAP. I use this method to identify the dynamics of E-cadherin at the cellular junctions of MDCK cells.

4.2 Results

To understand the dynamics of the vesicle mediated protein recycling, I modified the method of monitoring fluorescence recovery in FRAP. In our custom built confocal microscopy setup, I photobleached a small area along the intercellular junction (2x2 μm) and monitored the recovery by counting individual photon arrivals using an Avalanche Photodiode (APD). The APD triggers TTL pulses upon arrival of photons at a rate of ~11 M counts/s and I used a FPGA (Field Programable Gated Array) to record the TTL pulses at 80 MHz. This setup was built in our lab by Mr. Hussam Ibrahim and Mr. Patrick Schmidt which allowed us to count photons at ~100 ns intervals, which is orders of magnitudes higher than the temporal resolution of conventional FRAP. I used this method to monitor the dynamics of Ecads at the intercellular junctions.

In my experiments, I used Madin-Darby Canine Kidney (MDCK) cells expressing Ecads genetically modified with DsRed at the C-terminal. The cells were grown to confluency on a collagen coated coverslip for more than 24 hrs. First, a large area (50 μm x 50 μm) of the sample was scanned using 100 nW laser power (Figure 4.1A). Then I zoomed into a cell junction by scanning a small area (10 μm x 10 μm) and centered at a point on the junction (Figure 4.1 B). After collecting fluorescence signal for 10 s, to determine the pre-bleach ntensity, a small area (2 μm x 2 μm) was photo-bleached using 700 μW laser power lasting ~5 s (Figure 4.1C). The photobleached area was larger than the field of view. Subsequently, fluorescent recovery was monitored at a diffraction limited spot for 5 minutes (Figure 4.1D).

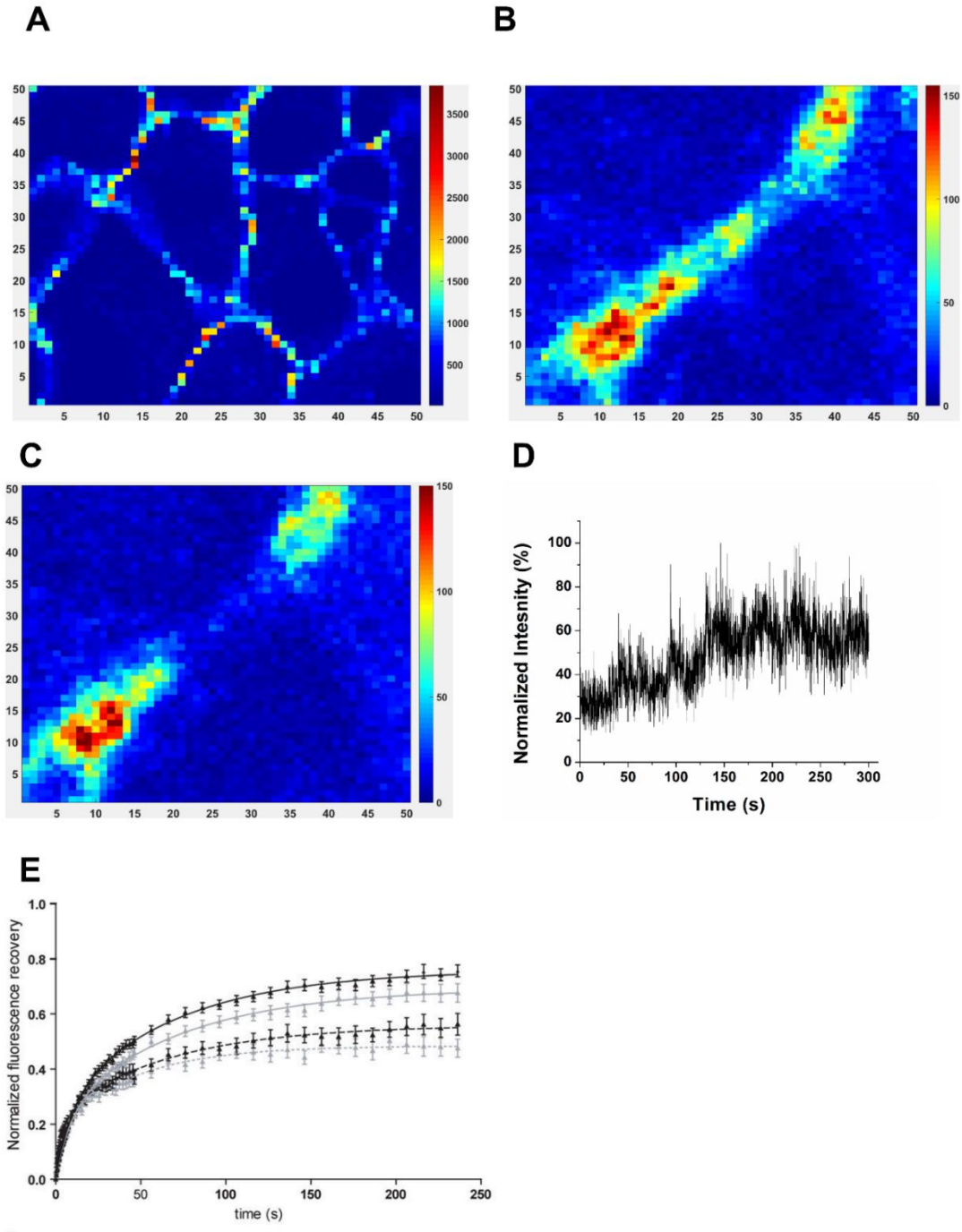

Figure 4.1: FRAP experiment is performed by scanning a (A) 50 µm x 50 µm area on a confluent MDCK cells expressing Ecad with DsRed. A junction is selected and zoomed in to (B) 10 µm x 10 µm area and a center for photobleaching is selected. (C) Scanned image after fluorescent recovery (10 µm x 10 µm) (D) fluorescent recovery at the center of (C), collected arrival of each photon by APD and binned at 100 ms. (E) Conventional FRAP data for Ecad adapted from Strale et al.

I first monitored the recovery for MDCK cells which showed a recovery similar to previously reported but with high fluctuations which cannot be detected in the conventional FRAP data (Figure 4.1E, example FRAP curve adapted from Strale et al [47]). To avoid focus drift, the objective was mounted on a CRISP autofocus system which maintains a constant focus. We have seen negligible drift in the xy plane in 5 minutes collection time. Thus, the fluctuations seen in the data are not caused by drift of the microscope. This was further confirmed by repeating the same FRAP experiment on a sample with fixed fluorescent streptavidin where no fluctuation was seen (data not shown). Hence, the fluctuations seen could be due to proteins fused by vesicles or other fluctuations from the cell.

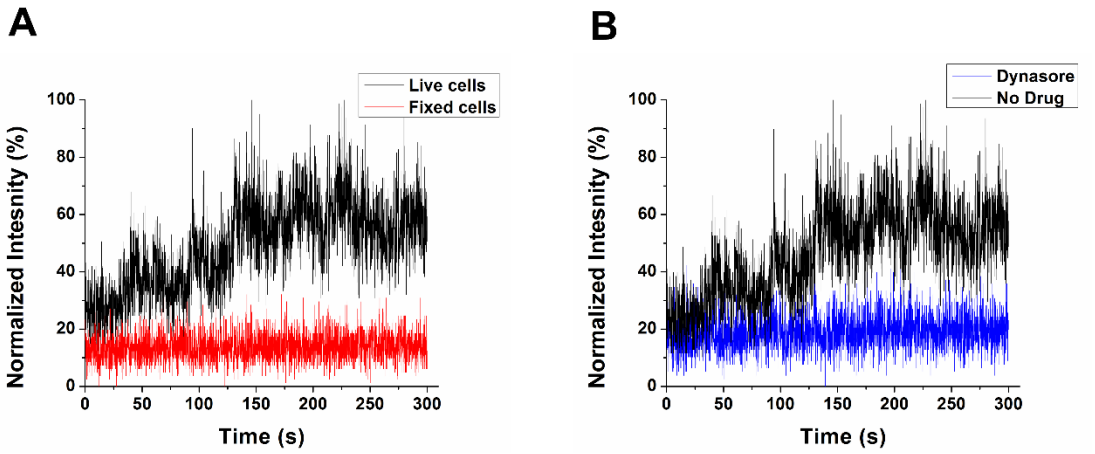

Figure 4.2: FRAP data for (A) live cells (black) and fixed cells (red) (B) cells with no dynasore (black) and with dynasore (blue)

Next, to confirm that the fluctuations in fluorescence recovery was due to cellular dynamics, we performed a FRAP experiment on MDCK cells that were fixed using treatment with 4% paraformaldehyde (Figure 4.2 A). No recovery or fluorescence fluctuations were measured with the fixed MDCK cells. To further confirm that these fluctuations were due to vesicles, I treated the cells with the pharmaceutical drug dynasore [48,49] that inhibits clathrin-dependent endocytosis (Figure 4.2B). In the dynasore treated cells, the fraction of fluorescence recovery was significantly smaller compared to the untreated cells. We also did

not see any fluctuations in the fluorescence recovery. These data show that the fluctuations seen on the FRAP collected at a faster rate are due to cellular dynamics controlled by exocytosis and endocytosis.

4.3 Discussion

Adherens junctions are formed by the interaction of cadherins from apposing cells. The cytoplasmic region of the cadherins are bound to catenins which link to the actin cytoskeleton. Our data shows that the adherens junctions are not static but are highly dynamic. The classical view is, that membrane diffusion plays a major role in the mobility and local regulation of density of cadherins in plasma membrane [15]. A second view is that cadherins are recycled in and out of the cells by endocytosis and exocytosis mainly mediated by vesicles[48]. Previous studies suggest that at initial stages of the contacts, membrane diffusion is prominent while in mature, established junctions endocytosis is mainly involved in recycling of the cadherins.

FRAP has been used to study the dynamics and kinetics of molecules. In conventional FRAP, data for faster dynamics is not available. I collected data with significantly higher time resolution than conventional FRAP and showed that fluctuations in fluorescence recovery may correspond to cadherins vesicles fusing at cell-cell contacts. Our data show that in the presence of dynasore, an endocytosis inhibitor, the fluorescence recovery and the fluctuations in fluorescence signals are significantly decreased. This indicates that at mature cell junctions, proteins are remodeled by the endocytosis not by membrane diffusions.

Fluorescence correlation spectroscopy (FCS), has been used to determine dynamic parameters such as diffusion, reaction or aggregation [50–53] and has been used to characterize endocytic pathways or clustering mechanisms at the onset of endocytosis [51,54]. These measurements exploit the fluorescence fluctuations induced by low numbers of diffusing labeled particles in a confocal setup to analyze their concentrations and mobilities. FCS can

be used to analyze FRAP data collected in this work. Furthermore, application of mechanical tugging force has been shown to trigger increases in the size of the adherens junctions[55]. It would be interesting to combine AFM with the current FRAP set up to test the dynamic coordination of mechanical forces and dynamic changes at cell-cell junctions.

4.4 Materials and Method

4.4.1 Cell culture

Madin-Darby Canine Kidney (MDCK) type II G cells, stably expressing Ecad tagged with DsRed were kind gift from Prof. W. James Nelson (Stanford University). Cells were grown to confluency in DMEM (Dulbecco's Modified Eagle's medium) with high glucose, 10 % FBS (Fetal bovine serum) and 1 % Penicillin-Streptomycin at 37 ˚C in 5% CO_2 incubator on a collagen coated coverslip for 24 -36 hrs. Dynasore (Sigma) was dissolved in DMSO and diluted to 60 µM in serum free DMEM. For fixing the cells, confluent monolayer was washed with PBS buffer, then incubated in 4% paraformaldehyde for 15 mints and washed again with PBS and imaged.

4.4.2 FRAP experimental set up

Coverslip with the cells was mounted on a custom designed confocal microscope [56]. A 532 nm laser beam was focused to a diffraction-limited spot on the glass coverslip using a 60x, 1.42 N.A., oil-immersion objective (Olympus) mounted on a CRISP autofocus system. For scanning, pre-bleach and recovery, 100 nW laser power was used while 700 µW was used to photo-bleach fluorescence. Emitted fluorescence was collected by the same objective and focused onto the detection face of a Single Photon Avalanche Diode (SPAD, Micro Photon Devices) that has a maximum count rate of 11.8 Mc/s. A bandpass filter was placed in front of the detector to transmit only the fluorescence from DsRed and to block the back-

scattered excitation light. Timestamps of TTL pulses, triggered by the arrival of individual photons on the SPAD, were recorded at 80 MHz by a field programmable gate array (FPGA, NI Instruments) using custom LabVIEW software.

4.5 References

1. Heisenberg, C.-P. & Bellaïche, Y. Forces in tissue morphogenesis and patterning. *Cell* **153,** 948–962 (2013).

2. Stepniak, E., Radice, G. L. & Vasioukhin, V. Adhesive and signaling functions of cadherins and catenins in vertebrate development. *Cold Spring Harb. Perspect. Biol.* **1,** a002949 (2009).

3. Kowalczyk, A. P. & Nanes, B. A. Adherens junction turnover: regulating adhesion through cadherin endocytosis, degradation, and recycling. *Subcell. Biochem.* **60,** 197–222 (2012).

4. Miller, J. R. & McClay, D. R. Characterization of the role of cadherin in regulating cell adhesion during sea urchin development. *Dev. Biol.* **192,** 323–339 (1997).

5. Oda, H., Tsukita, S. & Takeichi, M. Dynamic behavior of the cadherin-based cell-cell adhesion system during Drosophila gastrulation. *Dev. Biol.* **203,** 435–450 (1998).

6. Ogata, S. *et al.* TGF-beta signaling-mediated morphogenesis: modulation of cell adhesion via cadherin endocytosis. *Genes Dev.* **21,** 1817–1831 (2007).

7. Steinberg, M. S. & Takeichi, M. Experimental specification of cell sorting, tissue spreading, and specific spatial patterning by quantitative differences in cadherin expression. *Proc. Natl. Acad. Sci. USA* **91,** 206–209 (1994).

8. Hirohashi, S. Inactivation of the E-cadherin-mediated cell adhesion system in human cancers. *Am. J. Pathol.* **153,** 333–339 (1998).

9. Xie, L. *et al.* Altered expression of E-cadherin by hepatocyte growth factor and effect on the prognosis of nasopharyngeal carcinoma. *Ann. Surg. Oncol.* **17,** 1927–1936 (2010).

10. Brouxhon, S. *et al.* Sequential down-regulation of E-cadherin with squamous cell carcinoma progression: loss of E-cadherin via a prostaglandin E2-EP2 dependent posttranslational mechanism. *Cancer Res.* **67,** 7654–7664 (2007).

11. Lawler, K., O'Sullivan, G., Long, A. & Kenny, D. Shear stress induces internalization of E-cadherin and invasiveness in metastatic oesophageal cancer cells by a Src-dependent pathway. *Cancer Sci.* **100,** 1082–1087 (2009).

12. Sako, Y., Nagafuchi, A., Tsukita, S., Takeichi, M. & Kusumi, A. Cytoplasmic regulation of the movement of E-cadherin on the free cell surface as studied by optical tweezers and single particle tracking: corralling and tethering by the membrane skeleton. *J. Cell Biol.* **140,** 1227–1240 (1998).

13. Troyanovsky, R. B., Sokolov, E. P. & Troyanovsky, S. M. Endocytosis of cadherin from intracellular junctions is the driving force for cadherin adhesive dimer disassembly. *Mol. Biol. Cell* **17,** 3484–3493 (2006).

14. Cavey, M., Rauzi, M., Lenne, P.-F. & Lecuit, T. A two-tiered mechanism for stabilization and immobilization of E-cadherin. *Nature* **453,** 751–756 (2008).

15. Iino, R., Koyama, I. & Kusumi, A. Single molecule imaging of green fluorescent proteins in living cells: E-cadherin forms oligomers on the free cell surface. *Biophys. J.* **80,** 2667–2677 (2001).

16. Sako, Y. & Kusumi, A. Compartmentalized structure of the plasma membrane for receptor movements as revealed by a nanometer-level motion analysis. *J. Cell Biol.* **125,** 1251–1264 (1994).

17. Lambert, M., Choquet, D. & Mège, R.-M. Dynamics of ligand-induced, Rac1-dependent anchoring of cadherins to the actin cytoskeleton. *J. Cell Biol.* **157,** 469–479 (2002).

18. Troyanovsky, R. B., Sokolov, E. P. & Troyanovsky, S. M. Endocytosis of cadherin from intracellular junctions is the driving force for cadherin adhesive dimer disassembly. *Mol. Biol. Cell* **17,** 3484–3493 (2006).

19. Bryant, D. M. & Stow, J. L. The ins and outs of E-cadherin trafficking. *Trends Cell Biol.* **14,** 427–434 (2004).

20. D'Souza-Schorey, C. Disassembling adherens junctions: breaking up is hard to do. *Trends Cell Biol.* **15,** 19–26 (2005).

21. De Beco, S., Amblard, F. & Coscoy, S. New insights into the regulation of E-cadherin distribution by endocytosis. *Int. Rev. Cell Mol. Biol.* **295,** 63–108 (2012).

22. Ivanov, A. I., Nusrat, A. & Parkos, C. A. Endocytosis of the apical junctional complex: mechanisms and possible roles in regulation of epithelial barriers. *Bioessays* **27,** 356–365 (2005).

23. Kevil, C. G. *et al.* Role of cadherin internalization in hydrogen peroxide-mediated endothelial permeability. *Free Radic. Biol. Med.* **24,** 1015–1022 (1998).

24. Alexander, J. S., Jackson, S. A., Chaney, E., Kevil, C. G. & Haselton, F. R. The role of cadherin endocytosis in endothelial barrier regulation: involvement of protein kinase C and actin-cadherin interactions. *Inflammation* **22,** 419–433 (1998).

25. Le, T. L., Yap, A. S. & Stow, J. L. Recycling of E-cadherin: a potential mechanism for regulating cadherin dynamics. *J. Cell Biol.* **146,** 219–232 (1999).

26. Akhtar, N. & Hotchin, N. A. RAC1 regulates adherens junctions through endocytosis of E-cadherin. *Mol. Biol. Cell* **12,** 847–862 (2001).

27. Bryant, D. M. *et al.* EGF induces macropinocytosis and SNX1-modulated recycling of E-cadherin. *J. Cell Sci.* **120,** 1818–1828 (2007).

28. Paterson, A. D., Parton, R. G., Ferguson, C., Stow, J. L. & Yap, A. S. Characterization of E-cadherin endocytosis in isolated MCF-7 and chinese hamster ovary cells: the initial fate of unbound E-cadherin. *J. Biol. Chem.* **278,** 21050–21057 (2003).

29. Conner, S. D. & Schmid, S. L. Regulated portals of entry into the cell. *Nature* **422,** 37–44 (2003).

30. Chandrasekar, I. *et al.* Nonmuscle myosin II is a critical regulator of clathrin-mediated endocytosis. *Traffic* **15,** 418–432 (2014).

31. Lu, Z., Ghosh, S., Wang, Z. & Hunter, T. Downregulation of caveolin-1 function by EGF leads to the loss of E-cadherin, increased transcriptional activity of beta-catenin, and enhanced tumor cell invasion. *Cancer Cell* **4,** 499–515 (2003).

32. Parton, R. G. & Richards, A. A. Lipid rafts and caveolae as portals for endocytosis: new insights and common mechanisms. *Traffic* **4,** 724–738 (2003).

33. Amyere, M. *et al.* Origin, originality, functions, subversions and molecular signalling of macropinocytosis. *Int. J. Med. Microbiol.* **291,** 487–494 (2002).

34. Simões-Correia, J. *et al.* Endoplasmic reticulum quality control: a new mechanism of E-cadherin regulation and its implication in cancer. *Hum. Mol. Genet.* **17,** 3566–3576 (2008).

35. Tanjore, H. *et al.* Alveolar epithelial cells undergo epithelial-to-mesenchymal transition in response to endoplasmic reticulum stress. *J. Biol. Chem.* **286,** 30972–30980 (2011).

36. Deborde, S. *et al.* Clathrin is a key regulator of basolateral polarity. *Nature* **452,** 719–723 (2008).

37. Chen, Y.-T., Stewart, D. B. & Nelson, W. J. Coupling Assembly of the E-Cadherin/β-Catenin Complex to Efficient Endoplasmic Reticulum Exit and Basal-lateral Membrane Targeting of E-Cadherin in Polarized MDCK Cells. *J. Cell Biol.* **144,** 687–699 (1999).

38. Miranda, K. C. *et al.* A dileucine motif targets E-cadherin to the basolateral cell surface in Madin-Darby canine kidney and LLC-PK1 epithelial cells. *J. Biol. Chem.* **276,** 22565–22572 (2001).

39. Lock, J. G. & Stow, J. L. Rab11 in recycling endosomes regulates the sorting and basolateral transport of E-cadherin. *Mol. Biol. Cell* **16,** 1744–1755 (2005).

40. Ivanov, A. I. & Naydenov, N. G. Dynamics and regulation of epithelial adherens junctions: recent discoveries and controversies. *Int. Rev. Cell Mol. Biol.* **303,** 27–99 (2013).

41. He, B. & Guo, W. The exocyst complex in polarized exocytosis. *Curr. Opin. Cell Biol.* **21,** 537–542 (2009).

42. Jahn, R. & Scheller, R. H. SNAREs--engines for membrane fusion. *Nat. Rev. Mol. Cell Biol.* **7,** 631–643 (2006).

43. Malsam, J., Kreye, S. & Söllner, T. H. Membrane fusion: SNAREs and regulation. *Cell Mol. Life Sci.* **65,** 2814–2832 (2008).

44. Grindstaff, K. K. *et al.* Sec6/8 complex is recruited to cell-cell contacts and specifies transport vesicle delivery to the basal-lateral membrane in epithelial cells. *Cell* **93,** 731–740 (1998).

45. Langevin, J. *et al.* Drosophila exocyst components Sec5, Sec6, and Sec15 regulate DE-Cadherin trafficking from recycling endosomes to the plasma membrane. *Dev. Cell* **9,** 365–376 (2005).

46. Wu, X. *et al.* Clathrin exchange during clathrin-mediated endocytosis. *J. Cell Biol.* **155,** 291–300 (2001).

47. Strale, P.-O. *et al.* The formation of ordered nanoclusters controls cadherin anchoring to actin and cell-cell contact fluidity. *J. Cell Biol.* **210,** 333–346 (2015).

48. De Beco, S., Gueudry, C., Amblard, F. & Coscoy, S. Endocytosis is required for E-cadherin redistribution at mature adherens junctions. *Proc. Natl. Acad. Sci. USA* **106,** 7010–7015 (2009).

49. Macia, E. *et al.* Dynasore, a cell-permeable inhibitor of dynamin. *Dev. Cell* **10,** 839–850 (2006).

50. Bacia, K., Kim, S. A. & Schwille, P. Fluorescence cross-correlation spectroscopy in living cells. *Nat. Methods* **3,** 83–89 (2006).

51. Palmer, A. G. & Thompson, N. L. Fluorescence correlation spectroscopy for detecting submicroscopic clusters of fluorescent molecules in membranes. *Chem Phys Lipids* **50,** 253–270 (1989).

52. Sprague, B. L., Pego, R. L., Stavreva, D. A. & McNally, J. G. Analysis of binding reactions by fluorescence recovery after photobleaching. *Biophys. J.* **86,** 3473–3495 (2004).

53. Machán, R. & Hof, M. Lipid diffusion in planar membranes investigated by fluorescence correlation spectroscopy. *Biochim. Biophys. Acta* **1798,** 1377–1391 (2010).

54. Bacia, K., Majoul, I. V. & Schwille, P. Probing the endocytic pathway in live cells using dual-color fluorescence cross-correlation analysis. *Biophys. J.* **83,** 1184–1193 (2002).

55. Liu, Z., Tan, J. L., Cohen, D. M. & Yang, M. T. Mechanical tugging force regulates the size of cell–cell junctions. *National Acad Sciences*

56. Li, H., Yen, C.-F. & Sivasankar, S. Fluorescence axial localization with nanometer accuracy and precision. *Nano Lett* **12,** 3731–3735 (2012).

CHAPTER 5. CONCLUSIONS AND FUTURE DIRECTIONS

5.1 Conclusions

In this dissertation, I studied the role of different cadherins in cell adhesion and junction assembly using single molecule AFM force measurements and cell-based assays. The first part of the dissertation characterizes the different binding roles of desmosomal cadherins and how they assemble to form desmosomes. The second part uses FRAP to understand the dynamics of the classical cadherin mediated adherens junctions.

Dsc2 and Dsg2 isoforms, studied in this dissertation are the primary desmosomal cadherin isoforms in simple epithelia [2]. Mutations in these proteins cause many diseases like arrhythmogenic right ventricular cardiomyopathy (ARVC) [3]. I used single molecule force measurements (SMFS) using AFM to differentiate the binding properties of Dsc2 and Dsg2 and to understand how they are incorporated into desmosomes. My SMFS results indicated that Dsc2 forms homophilic interactions in the presence of Ca^{2+}, and heterophilic interactions with Dsg2 independent of Ca^{2+}. In contrast, Dsg2 is involved only in heterotypic binding. My collaborators used micro-patterned substrates to confirm that Dsc2, but not Dsg2, was necessary and sufficient to induce the recruitment of a desmosome-specific cytoplasmic protein desmoplakin (DP) into punctate cellular structures. Interestingly, the W2A mutation in Dsc2 inhibited Ca^{2+} dependent homophilic binding and the Dsc2W2A mutant appeared to be excluded from endogenous desmosomes in MDCK cells. This shows that Dsc2 homophilic binding occurs via a Ca^{2+} and W2 (strand-swap dimer) dependent mechanism. In contrast, the W2A mutation in Dsg2 affected neither Ca^{2+} independent heterophilic binding to Dsc2 in SMFS nor co-localization with endogenous desmosome puncta in MDCK cells. These results indicate that Dsg2 incorporation into desmosome occurs via a Ca^{2+} and W2 (strand swap dimer) independent mechanism that relies on heterophilic interactions and/or cytoplasmic interactions with other proteins in the desmosome.

In third Chapter, I asked the question how Dsgs are incorporated into desmosome?. Previous cell based studies have shown that the absence of classical cadherins delay desmosome formation [5–9]. I used AFM force measurements to resolve the roles of Ecad, Dsg2 and Dsc2 in desmosome assembly. AFM force measurements revealed that Ecad interacts with Dsg2 via a conserved Leu 175 on the Ecad *cis* binding interface. Using dynamic force spectroscopy, I also showed that the interactions between Dsc2:Dsg2 are longer lived than Dsc2 homodimer or Ecad:Dsg2. Our collaborators used SIM imaging to demonstrate that while Ecad is present in nascent desmosomes, it is excluded as desmosomes mature. Our collaborators also used confocal imaging to reveal that desmosome assembly is initiated at sites of Ecad *trans* homodimerization and that Ecad-L175 is required for efficient Dsg2 and DP recruitment. Hence, we propose that Ecad *trans* interactions at nascent cell-cell contacts initiate the recruitment of Dsg2 through direct *cis* interactions with Ecad and then Dsg2 binds to Dsc2 to form robust desmosomes.

In Chapter four, I used fluorescence recovery after photobleaching (FRAP) with a custom built confocal microscopy which can detect arrival of single photons to study the dynamics of the Ecads in adherens junction. These measurements enabled us to distinguish fast dynamics that occur in the μs timescale compared to conventional FRAP, which can only identify dynamics on the second timescales. My experiments showed that adherens junctions are not static structures; rather, they undergo constant rearrangements. Previous publications [10–14] suggested that this can happen either due to exchange between pools of free monomers and *trans* dimers constrained to adhesion cites by the cytoskeleton, or by internalizing proteins by endocytosis and introducing new proteins into the junction by exocytosis. When endocytosis was blocked using the pharmaceutical agent dynasore, recovery of fluorescence was abolished, suggesting the recovery of fluorescence from newly introduced Ecads was due to vesicle fusion. All the studies that have shown membrane diffusion of Ecads are carried out on early junctions suggesting that Ecad membrane diffusion could be a prominent process

in early stages of the junction formation. However, as junctions mature the monomer pool might be reduced and endocytosis may become the major mechanism for cadherin trafficking. More controlled experiments using mutants are needed to decouple the roles of diffusion and vesicle trafficking in cadherin recycling in cells.

5.2 Future Directions

My research on desmosomal cadherins identifies important roles of different cadherins in desmosome assembly. On the cellular level, these proteins are co-expressed and involved in many signaling pathways, which makes it difficult to assign a unique functional role for each cadherin in cells. Our approach using single molecule AFM measurements in cell-free systems, eliminates this ambiguity. Hence, we plan to use this approach to study other isoforms of Dscs and Dsgs.

My studies also identified that Dsc2 interact homophilically using a conserved W2 amino acid. I also showed that Ecad interacts with Dsg2 using a conserved L175 on Ecad. However, the amino acids on Dsg2 that mediate binding to Ecad and to Dsc2 are unknown. Finding the Dsg2 binding interface through domain deletion and mutations would unravel the complete picture of the desmosome assembly.

Interestingly, confocal imaging of keratinocytes expressing L175 Ecad showed that these cells did not recruit DP or Dsg2. Since keratinocytes express Dsg3 which should have recruited DP, the L175 Ecad mediated dimerization could be a common mechanism for other Dsgs too. Identifying if Ecad and Dsg3 bind, would be important to fully understand desmosome assembly.

Previously our lab has characterized how Ecads change their adhesion in response to pulling forces by forming catch, slip and ideal bonds [15–17]. Similar measurements with Dsc and Dsg will reveal how these cadherins respond to pulling forces.

Finally, cells are constantly exposed to mechanical stress which influence the dynamics of cell-cell junctions. Combining AFM with the confocal microscopy will allow us to

understand the changes to the dynamics of the cadherins in intercellular junctions in the presence of force. The force sensed by the cadherin extracellular region is transmitted to the cytoplasm and is known to activate biochemical signals within the cells [19,20]. It is widely accepted that α-catenin bound to the cadherin-β-catenin complex bridges cadherin to actin [21–26] and the binding of α-catenin to β-catenin and actin requires force [27,28]. In the presence of tension, α-catenin undergoes conformational changes which results in the recruitment of many other proteins such as vinculin to the site of force application [29,30] . Hence, breaking the Ecad-catanin-actin linkage by mutations and determining how that influences the cell-cell junction dynamics will provide fundamental insights into how cells sense and respond to mechanical forces.

5.3 References

1. Hatzfeld, M., Keil, R. & Magin, T. M. Desmosomes and intermediate filaments: their consequences for tissue mechanics. *Cold Spring Harb. Perspect. Biol.* **9,** (2017).

2. Dusek, R. L., Godsel, L. M. & Green, K. J. Discriminating roles of desmosomal cadherins: beyond desmosomal adhesion. *J. Dermatol. Sci.* **45,** 7–21 (2007).

3. Murray, B. Arrhythmogenic right ventricular dysplasia/cardiomyopathy (ARVD/C): a review of molecular and clinical literature. *J Genet Couns* **21,** 494–504 (2012).

4. Mazurek, S. & Kim, G. H. Genetic and epigenetic regulation of arrhythmogenic cardiomyopathy. *Biochim. Biophys. Acta* **1863,** 2064–2069 (2017).

5. Amagai, M. *et al.* Delayed assembly of desmosomes in keratinocytes with disrupted classic-cadherin-mediated cell adhesion by a dominant negative mutant. *J. Invest. Dermatol.* **104,** 27–32 (1995).

6. Lewis, J. E., Jensen, P. J. & Wheelock, M. J. Cadherin function is required for human keratinocytes to assemble desmosomes and stratify in response to calcium. *J. Invest. Dermatol.* **102,** 870–877 (1994).

7. Gumbiner, B., Stevenson, B. & Grimaldi, A. The role of the cell adhesion molecule uvomorulin in the formation and maintenance of the epithelial junctional complex. *J. Cell Biol.* **107,** 1575–1587 (1988).

8. Wheelock, M. J. & Jensen, P. J. Regulation of keratinocyte intercellular junction organization and epidermal morphogenesis by E-cadherin. *J. Cell Biol.* **117,** 415–425 (1992).

9. Michels, C., Buchta, T., Bloch, W., Krieg, T. & Niessen, C. M. Classical Cadherins Regulate Desmosome Formation. *J Investig Dermatol* **129,** 2072–2075 (2009).

10. Ivanov, A. I. & Naydenov, N. G. Dynamics and regulation of epithelial adherens junctions: recent discoveries and controversies. *Int. Rev. Cell Mol. Biol.* **303,** 27–99 (2013).

11. De Beco, S., Perney, J.-B., Coscoy, S. & Amblard, F. Mechanosensitive Adaptation of E-Cadherin Turnover across adherens Junctions. *PLoS One* **10,** e0128281 (2015).

12. Iino, R., Koyama, I. & Kusumi, A. Single molecule imaging of green fluorescent proteins in living cells: E-cadherin forms oligomers on the free cell surface. *Biophys. J.* **80,** 2667–2677 (2001).

13. Sako, Y., Nagafuchi, A., Tsukita, S., Takeichi, M. & Kusumi, A. Cytoplasmic regulation of the movement of E-cadherin on the free cell surface as studied by optical tweezers and single particle tracking: corralling and tethering by the membrane skeleton. *J. Cell Biol.* **140,** 1227–1240 (1998).

14. Sako, Y. & Kusumi, A. Compartmentalized structure of the plasma membrane for receptor movements as revealed by a nanometer-level motion analysis. *J. Cell Biol.* **125,** 1251–1264 (1994).

15. Rakshit, S., Zhang, Y., Manibog, K., Shafraz, O. & Sivasankar, S. Ideal, catch, and slip bonds in cadherin adhesion. *Proc. Natl. Acad. Sci. USA* **109,** 18815–18820 (2012).

16. Manibog, K., Li, H., Rakshit, S. & Sivasankar, S. Resolving the molecular mechanism of cadherin catch bond formation. *Nat Commun* **5,** 3941 (2014).

17. Manibog, K. *et al.* Molecular determinants of cadherin ideal bond formation: Conformation-dependent unbinding on a multidimensional landscape. *Proc. Natl. Acad. Sci. USA* **113,** E5711–20 (2016).

18. Liu, Z. *et al.* Mechanical tugging force regulates the size of cell-cell junctions. *Proc. Natl. Acad. Sci. USA* **107,** 9944–9949 (2010).

19. Gumbiner, B. M. Regulation of cadherin adhesive activity. *J. Cell Biol.* **148,** 399–404 (2000).

20. Lecuit, T. & Yap, A. S. E-cadherin junctions as active mechanical integrators in tissue dynamics. *Nat. Cell Biol.* **17,** 533–539 (2015).

21. Ozawa, M., Baribault, H. & Kemler, R. The cytoplasmic domain of the cell adhesion molecule uvomorulin associates with three independent proteins structurally related in different species. *EMBO J.* **8,** 1711–1717 (1989).

22. Pokutta, S. & Weis, W. I. Structure of the dimerization and beta-catenin-binding region of alpha-catenin. *Mol. Cell* **5,** 533–543 (2000).

23. Huber, A. H. & Weis, W. I. The Structure of the β-Catenin/E-Cadherin Complex and the Molecular Basis of Diverse Ligand Recognition by β-Catenin. *Cell* **105,** 391–402 (2001).

24. Rimm, D. L., Koslov, E. R., Kebriaei, P., Cianci, C. D. & Morrow, J. S. al(E)-Catenin is an actin-binding and -bundling protein mediating. *PNAS* **92,** 8813–8817 (1995).

25. Pokutta, S., Drees, F., Takai, Y., Nelson, W. J. & Weis, W. I. Biochemical and structural definition of the l-afadin- and actin-binding sites of alpha-catenin. *J. Biol. Chem.* **277,** 18868–18874 (2002).

26. Nagafuchi, A. & Takeichi, M. Cell binding function of E-cadherin is regulated by the cytoplasmic domain. *EMBO J.* **7,** 3679–3684 (1988).

27. Drees, F., Pokutta, S., Yamada, S., Nelson, W. J. & Weis, W. I. Alpha-catenin is a molecular switch that binds E-cadherin-beta-catenin and regulates actin-filament assembly. *Cell* **123,** 903–915 (2005).

28. Yamada, S., Pokutta, S., Drees, F., Weis, W. I. & Nelson, W. J. Deconstructing the cadherin-catenin-actin complex. *Cell* **123,** 889–901 (2005).

29. Yonemura, S., Wada, Y., Watanabe, T., Nagafuchi, A. & Shibata, M. alpha-Catenin as a tension transducer that induces adherens junction development. *Nat. Cell Biol.* **12,** 533–542 (2010).

30. Kim, T.-J. *et al.* Dynamic visualization of α-catenin reveals rapid, reversible conformation switching between tension states. *Curr. Biol.* **25,** 218–224 (2015).

.